Available online at www.sciencedirect.com
SCIENCE DIRECT®
Journal of Sound and Vibration 294 (2006) 23–48
JOURNAL OF SOUND AND VIBRATION
www.elsevier.com/locate/jsvi

Dynamic model of ball bearings with internal clearance and waviness

Bai Changqing*, Xu Qingyu

Department of Engineering Mechanics, School of Aerospace, Xi'an Jiaotong University, Xi'an 710049, PR China

Received 3 August 2004; received in revised form 1 August 2005; accepted 15 October 2005
Available online 4 January 2006

Abstract

In this paper, a general dynamic model is presented for studying the dynamic properties of rotor system supported by ball bearings under the effects of both internal clearance and bearing running surface waviness. The ball bearing model includes the high-speed effects of ball centrifugal force and gyroscopic moment. The cage speed is considered a time-variation parameter related with the orbital speed of balls. Numerical results of this research are in good agreement with prior authors' experimental researches and already existing models. Then the model is employed to investigate the effects of clearance, waviness, preload and radial force on the nonlinear stability and vibration behavior of a rotor bearing system at high speed. It is shown that the clearance, axial preload and radial force play a significant role in affecting the system stability. The effect of outer race waviness on cage speed variation is more considerable than that of inner race and ball waviness.

1. Introduction

Ball bearings are of great importance in numerous rotating machinery systems. They have widely been used in high-speed spindle systems including aircraft gas turbines and rocket motors, due to the requirements for high reliability and low power consumption. As demands on running accuracy and speed are increased, vibration analysis of rotors supported by ball bearings is becoming more and more important. Ball bearings, as one of sources of vibration, have attracted substantial attention because of their nonlinearity effects due to the Hertzian force deformation relationship, the varying compliance, the internal clearance, the waviness and so on. This situation creates considerable interest in analytical modeling of the bearing characteristics.

The effect on bearing static equilibrium of varying compliance was first studied by Perret [1] and Meldau [2]. Jones [3] proposed a quasi-static equilibrium model considering the effect of the centrifugal force and gyroscopic moment of ball. The proposed model was generalized by Harris [4]. Dynamic effects of varying compliance were investigated by Walters [5] who simulated the motion of the cage. Following his work, Gupta [6] developed a dynamic model for both ball and cylindrical roller bearings. He pointed out that the dynamic model eliminates most of the problems in the quasi-static model and provides a significant reduction in the

*Corresponding author. Tel.: +86 29 82663093.
E-mail address: bai_chq@sohu.com (B. Changqing).

0022-460X/$ - see front matter © 2005 Elsevier Ltd. All rights reserved.
doi:10.1016/j.jsv.2005.10.005

Nomenclature

A	amplitude of waviness in radial direction (m)
B	amplitude of waviness in axial direction (m)
C	amplitude of the ball waviness (m)
c	clearance (m)
D_b	ball diameter (m)
D_p	pitch diameter (m)
e	rotor mass eccentricity (m)
F	force (N)
$\{F\}$	bearing force vector (N) or (N m)
$\{f\}$	force function vector (N) or (N m)
g	forces equilibrium function
I	mass moment of inertia (kg m^2)
K	load-deflection constant for point contact (N m$^{-1.5}$)
L	nominal distance between rolling element center and race center of curvature (m)
l	actual distance between rolling element center and race center of curvature (m)
M	moment (N m)
m	mass (kg)
$[m]$, $[k]$, $[d]$	system mass, stiffness and damping + gyroscopic matrices
N	number of rolling elements
n	waviness order
P	external load (N)
p	radial waviness (m)
Q	contact force (N)
$\{Q\}$	contact force vector of rolling element (N)
q	axial waviness (m)
r	race radius of curvature (m)
(T)	transformation matrix $\{U\} \rightarrow \{u\}$ (m)
t	time (s)
$\{U\}$	displacement vector of bearing center $\{x\ y\ z\ \theta_x\ \theta_y\}^{\mathrm{T}}$ (m) or (rad)
$\{U\}$	displacement vector of inner race center of curvature $\{u_r\ u_z\ u_\phi\}$ (m) or (rad)
v	rolling element displacement (m)
w	ball waviness (m)
$\{X\}$	displacement vector of system DOF (m) or (rad)
α	contact angle (rad)
β	angle between ball rotational axis and bearing centerline (rad)
γ	D_b/D_p
Δt	time increment (s)
$\{\Delta W\}$	relative waviness vector (m)
δ	contact deformation or deflection (m)
ζ	initial phase angle of ball waviness (rad)
η	initial phase angle of axial waviness (rad)
λ	constant determined by the race control theory
ξ	initial phase angle of radial waviness (rad)
φ	angular location of rolling element (rad)
χ	identification parameter for contact
ψ	angular location (rad)
ω	angular velocity, shaft angular velocity (rad/s)

Subscripts

b	rolling element
c	cage
e	centrifugal
g	gyroscopic
i	inner race
j	rolling element index
m	ball orbital
n	waviness order
o	outer race
p	bearing center to nominal inter race center of curvature
r, z, ϕ	r, z, ϕ axes
x, y, z	x, y, z axes
0	nominal

overall design costs. Therefore, various nonlinear factors, bearing clearance and waviness especially, have drawn much attention in order to obtain the effective dynamic property of rotor bearing systems.

Clearance between the balls and the bearing races is essential to ball bearings. Much work has been carried out on its nonlinearity effects. The experimental studies of Gustafsson et al. [7] showed that clearance is an important parameter for ball passage vibrations. Yamamoto [8] presents an analytical model to investigate the vibrations of a vertical rotor supported by ball bearings with radial clearance. Childs [9] studied the effect of non-symmetric clearance on rotor motion with the aid of perturbation method. Saito [10] investigated the effect of radial clearance in an unbalanced Jeffcott rotor using the numerical harmonic balance technique.

Several researchers have employed two-degree-of-freedom (2dof) dynamic models performing the nonlinear simulation under the effect of clearance [11–14]. Mevel and Guyader [11] described different routes to chaos by varying a control parameter. Tiwari et al. [12] studied the nonlinear behaviors of a balanced rotor due to the effect of internal clearance of the ball bearing, and an unbalance rotor was analyzed in Ref. [13]. Harsha et al. [14] simulated some dynamic response of rotor supported by ball bearings, using a 2dof model with clearance and waviness. However, the 2dof models would not be accurate enough to perform the dynamic prediction of rotor bearing systems when the bearings are loaded and displaced in five degrees of freedom. De Mul et al. [15] presented a five-degree-of-freedom (5dof) model for calculation of the equilibrium and associated load distribution in ball bearings. Bearing clearance and centrifugal force of ball were considered in their research. Liew et al. [16] summarized 2dof and 5dof models with clearance, and illustrated the effect of ball centrifugal force. They indicated that the significant effect of 5dof model is noticed at high speeds and light preloads.

On the other hand, many researchers have studied the vibrations caused by waviness of ball bearings. Gustafsson et al. [7] studied the effect of not only clearance but also waviness and point out that low-order outer ring waviness affects the amplitudes of vibrations at the ball passage frequency. Tallian and Gustafsson [17] presented a linearized dynamic model analyzing the vibration caused by waviness. Yhland [18] examined the correspondence between waviness and the resulting vibration spectrum. Wardle and Poon [19] reported that the waviness produces most of the severe vibrations and noise problem in bearings. Later Wardle theoretically [20] and experimentally [21] studied the relation between the frequencies harmonic of waviness and bearing dynamic performance. A linear model was developed for the vibrations of a shaft bearing system caused by waviness in Ref. [22]. The model is valid for low and medium speeds on account of neglected centrifugal action of ball. Aktüuk [23] employed a 3dof dynamic model to simulate the radial and axial vibrations of a rigid shaft supported by ball bearings, and the effect of bearing waviness on the vibration of the shaft was investigated.

Jang and Jeong [24] proposed the 5dof excitation model of ball bearing waviness to investigate bearing vibration. Then considering the centrifugal force and gyroscopic moment of ball, they developed an analytical method to calculate the characteristics of the ball bearing under the effect of waviness in Ref. [25]. But they did not consider the effect of internal clearance, which might play an important role in the transient dynamic analysis of rotor supported by ball bearings. Otherwise the dynamic property of rotor was not taken into account and the time variation of cage angular velocity was not introduced into the numerical procedure.

Although many researchers have investigated the characteristics of ball bearings due to the effect of internal clearance or waviness, no studies have been published on dynamic analysis of ball bearings with both internal clearance and waviness considering 5dof. Hence, this paper will present a 5dof dynamic model to study the dynamic performance of ball bearings due to the effect of both internal clearance and waviness at high speed, where the centrifugal force and gyroscopic moment from balls should be taken into account. Furthermore, the cage speed will be considered a time-variation parameter related with the orbital speed of balls. Numerical results obtained from the proposed model will be validated with prior authors' experimental results and already existing models. Then the system stability and dynamic characteristics of a rotor bearing system will be investigated under the effects of internal clearance, waviness, axial preload and radial load.

2. Dynamic model

In order to investigate the dynamic characteristics of a rotor bearing system, the nonlinear bearing forces have to be determined first, and then the differential equations of motion for the system can be formulated.

2.1. Coordinate systems and transformations

Two sets of coordinate systems, as shown in Fig. 1, are defined for the purpose of numeric analysis. The inertial coordinate system (x, y, z), which is fixed in space, is a convenient orthogonal set of coordinates with the origin at the bearing (inner race) center. The z-axis is along the bearing rotational axis. The local rolling element coordinate system (r, Z, ϕ), with the same z-axis and origin at the nominal position of the inner race center of curvature, is fixed in the rolling element.

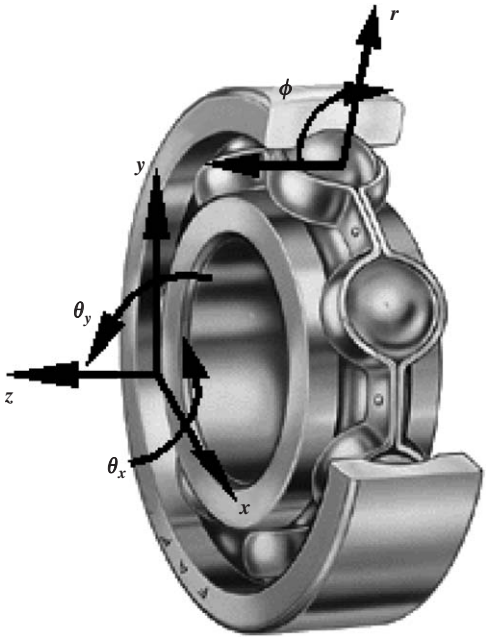

Fig. 1. Bearing coordinate systems.

For simplifying the expression in this paper, it is defined that the blank superscript referring to the variable indicates a time of t.

The general motion and load of the bearings can be completely described in 5dof. Thus, the displacement vector of the bearing center can be defined in the inertial coordinate system with respect to the mass center of the rotor. The vector, with components of the translation motions x,y,z and the angular displacements θ_x, θ_y, can be written as

$$\{U\} = \{x \quad y \quad z \quad \theta_x \quad \theta_y\}^{\mathrm{T}}. \tag{1}$$

The rolling element can be located with the displacement vector of the inner race center of curvature in the local rolling element coordinate system. For the jth ball, the displacement vector can be expressed as

$$\{u_j\} = \{u_{rj} \quad u_{zj} \quad u_{\phi j}\}^{\mathrm{T}}. \tag{2}$$

With the small motion assumption, the relationship between $\{u_j\}$ and $\{U\}$ is as follows:

$$\{u_j\} = [T_j]\{U\} + \{\Delta W_j\}, \tag{3}$$

where $[T_j]$ is transformation matrix

$$[T_j] = \begin{bmatrix} \cos\varphi_j & \sin\varphi_j & 0 & -(z_p + q_{ij})\sin\varphi_j & (z_p + q_{ij})\cos\varphi_j \\ 0 & 0 & 1 & (r_p + p_{ij})\sin\varphi_j & -(r_p + p_{ij})\cos\varphi_j \\ 0 & 0 & 0 & -\sin\varphi_j & \cos\varphi_j \end{bmatrix} \tag{4}$$

and $\{\Delta W_j\}$ is the relative waviness vector of the inner and outer races:

$$\{\Delta W_j\} = \{(p_{ij} - p_{oj}) \quad (q_{ij} - q_{oj}) \quad 0\}^{\mathrm{T}}. \tag{5}$$

This transformation relation is more general than that expressed in Refs. [15,16] where the waviness was left out of account. The angular location of the jth rolling element (Fig. 2) can be obtained by

$$\varphi_j = \frac{2\pi(j-1)}{N} + \psi_c + \varphi_0. \tag{6}$$

It was assumed that the cage angular velocity is an invariable in Refs. [16,25]. Then the angular location of the cage, ψ_c, is taken to be linear in time. However, this assumption is inappropriate as the clearance and waviness are taken into account. According to the intercoordination between the cage motion and balls motion, the

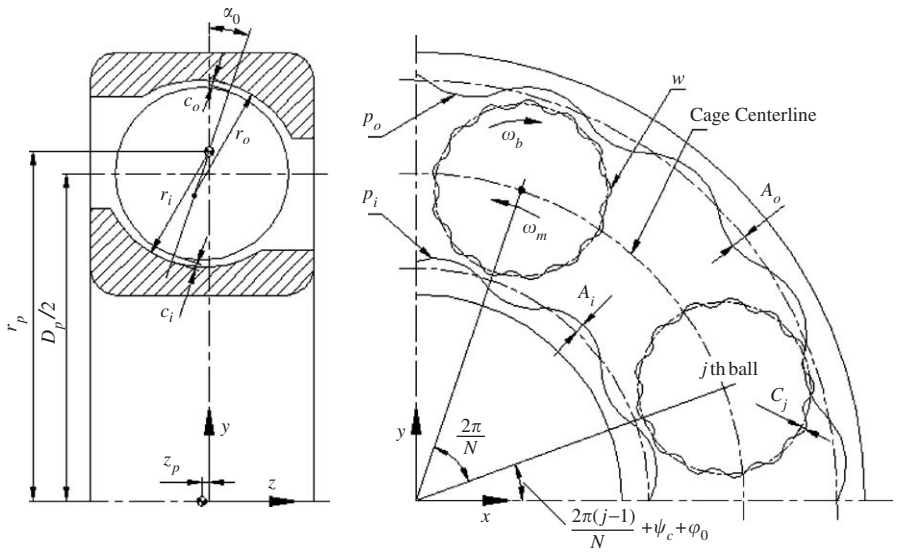

Fig. 2. Bearing geometry and waviness model.

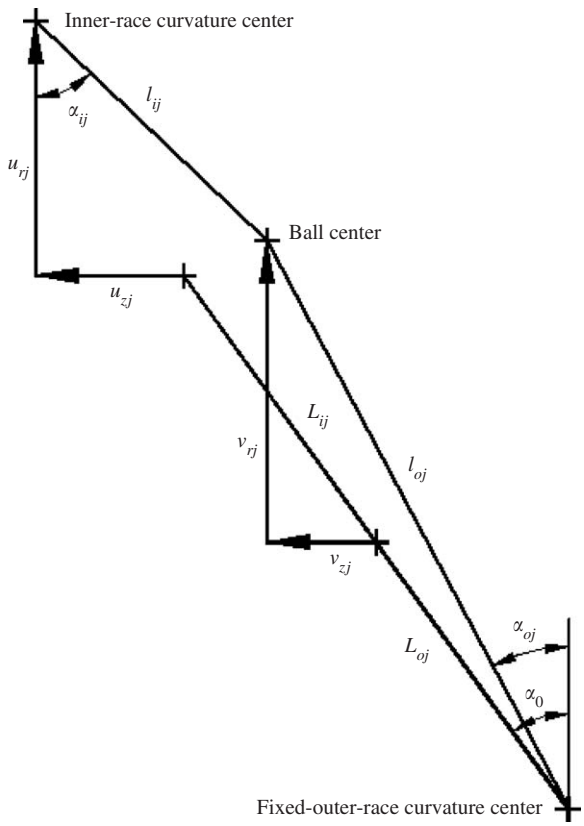

Fig. 3. Positions and displacements of race-curvature centers and ball center [16].

cage speed can be determined by the mean value of orbital angular velocities of balls that have contact with the inner race, as shown below.

$$\omega_c = \sum_{j=1}^{N} \chi_{ij}\omega_{mj} \Big/ \sum_{j=1}^{N} \chi_{ij}. \tag{7}$$

Thus, the angular location of the cage can be expressed as an incremental form:

$$\psi_c^{t+\Delta t} = \psi_c^t + \omega_c^t \cdot \Delta t. \tag{8}$$

2.2. Waviness model

The geometrical imperfections are often called waviness if its wavelength is much longer than the Hertzian contact width. As a source of vibration, waviness should be considered in modeling.

If it is assumed that the waviness of periodic lobes is described as a sinusoidal function, the localized defects could be expressed by the superposition of the several sinusoidal functions appropriately [24]. Note that the cage angular velocity is a time varying parameter. Then the radial waviness of the inner and outer race, as shown in Fig. 2, can be expressed as

$$p_{ij} = \sum_{n=1}^{\infty} A_{in} \cos[n(\psi_c - \omega_i t) + 2\pi(j-1)/N + \xi_{in}], \tag{9}$$

$$p_{oj} = \sum_{n=1}^{\infty} A_{on} \cos[n(\psi_c - \omega_o t) + 2\pi(j-1)/N + \xi_{on}] \tag{10}$$

and the axial waviness of the inner and outer race can be expressed as follows:

$$q_{ij} = \sum_{n=1}^{\infty} B_{in} \cos[n(\psi_c - \omega_i t) + 2\pi(j-1)/N + \eta_{in}], \tag{11}$$

$$q_{oj} = \sum_{n=1}^{\infty} B_{on} \cos[n(\psi_c - \omega_o t) + 2\pi(j-1)/N + \eta_{on}]. \tag{12}$$

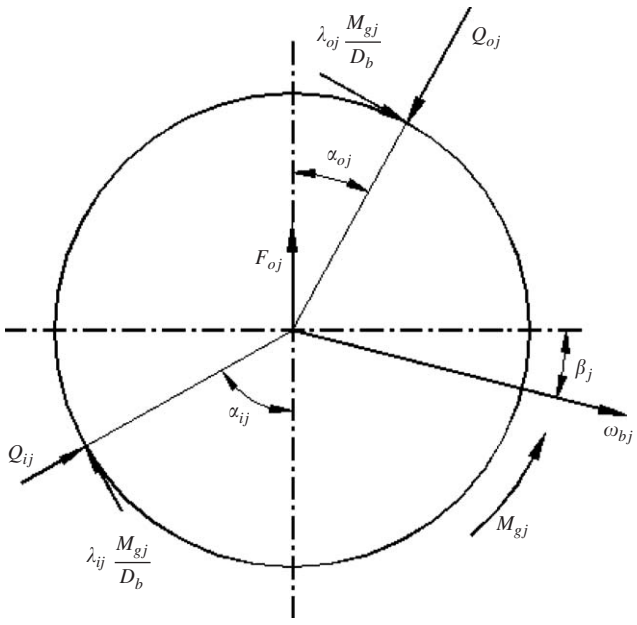

Fig. 4. Ball forces and moments [4].

If the angle difference of two contact points, where the ball is in contact with the inner and outer race respectively, is 180°, the ball waviness in contact with the inner and outer race (Fig. 2) can be given by

$$w_{ij} = \sum_{n=1}^{\infty} C_{nj} \cos(n\psi_{bj} + \zeta_{nj}), \tag{13}$$

$$w_{oj} = \sum_{n=1}^{\infty} C_{nj} \cos[n(\psi_{bj} + \pi) + \zeta_{nj}], \tag{14}$$

Table 1
Specification of ball bearing

Parameter	Value
Number of balls, N	18
Ball diameter, D_b	19.05 mm
Pitch diameter, D_p	140 mm
Inner race curvature radius, r_i	10.2870 mm
Outer race curvature radius, r_o	9.906 mm
Nominal contact angle, α_0	25°
Inner race clearance, c_i	0.004 mm
Outer race clearance, c_o	0.004 mm

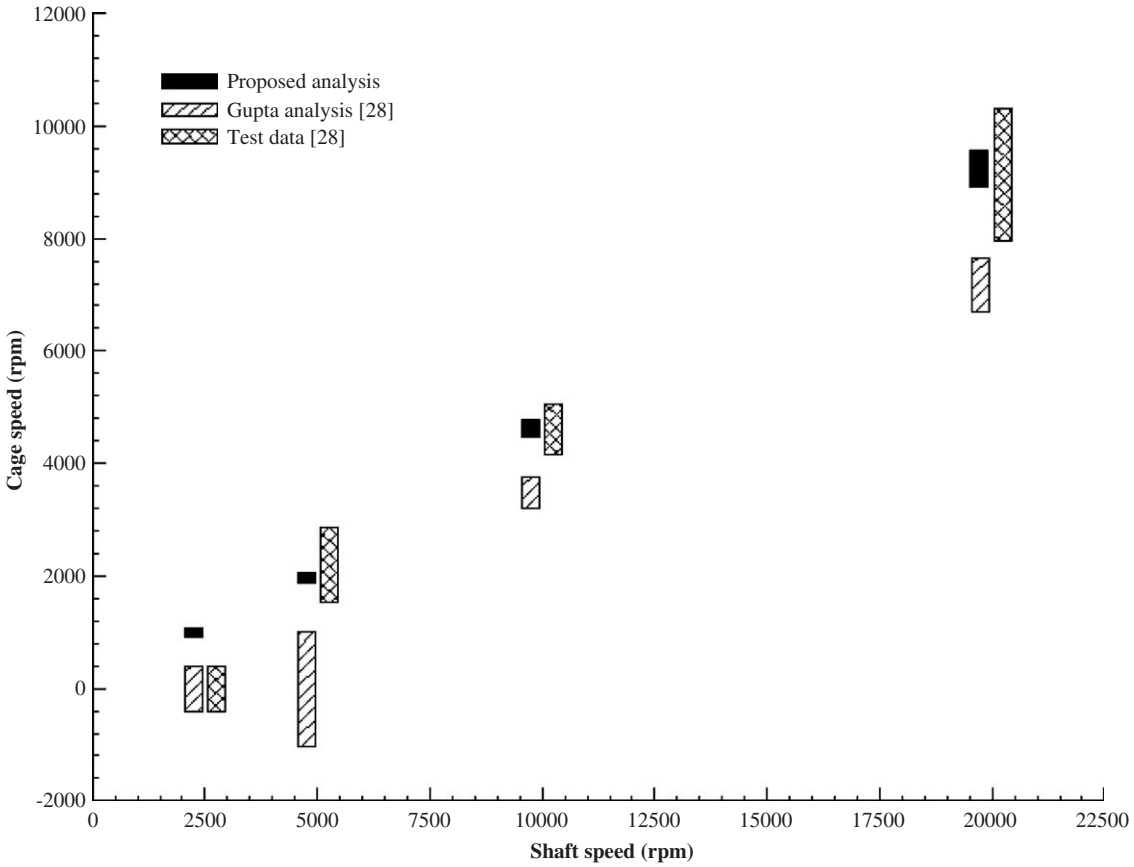

Fig. 5. The predicted cage speed compared to the speed determined from the test data and Gupta analysis [28].

where the angular location of the jth ball can be calculated from

$$\psi_{bj}^{t+\Delta t} = \psi_{bj}^{t} + \omega_{bj}^{t} \cdot \Delta t, \tag{15}$$

which is analogous to Eq. (8).

2.3. Ball equilibrium

Assume that the outer race is stationary and the inner race is displaced under the bearing loading, as shown in Fig. 3. Then the kinematic constraint and force equilibrium equations of a ball can be formulated as in this section. For a stationary inner race and a rotating outer race or simultaneous rotation of the outer and inner races, similar formulas can also be expressed.

Consider the effect of internal clearance, waviness and ball oversize. In the nominal situation ($\{U\} = \{0\}$), the distances between the ball center, and the inner and outer race centers of curvature, respectively, can be given by

$$L_{ij} = r_i - (D_b + h_j)/2 - w_{ij} - c_i, \tag{16}$$

$$L_{oj} = r_o - (D_b + h_j)/2 - w_{oj} - c_o. \tag{17}$$

In high-speed operation of ball bearings, the centrifugal forces and gyroscopic moment of ball are significant and must be considered in analysis. The inner and outer race contact angles are no longer equal because of the body forces resulting from the ball's motion, as shown in Fig. 3. The geometric relationships can be written as follows:

$$\tan \alpha_{ij} = \frac{L_{ij} \sin \alpha_0 + u_z - v_z}{L_{ij} \cos \alpha_0 + u_r - v_r}, \tag{18}$$

$$\tan \alpha_{oj} = \frac{L_{oj} \sin \alpha_0 + v_z}{L_{oj} \cos \alpha_0 + v_r}, \tag{19}$$

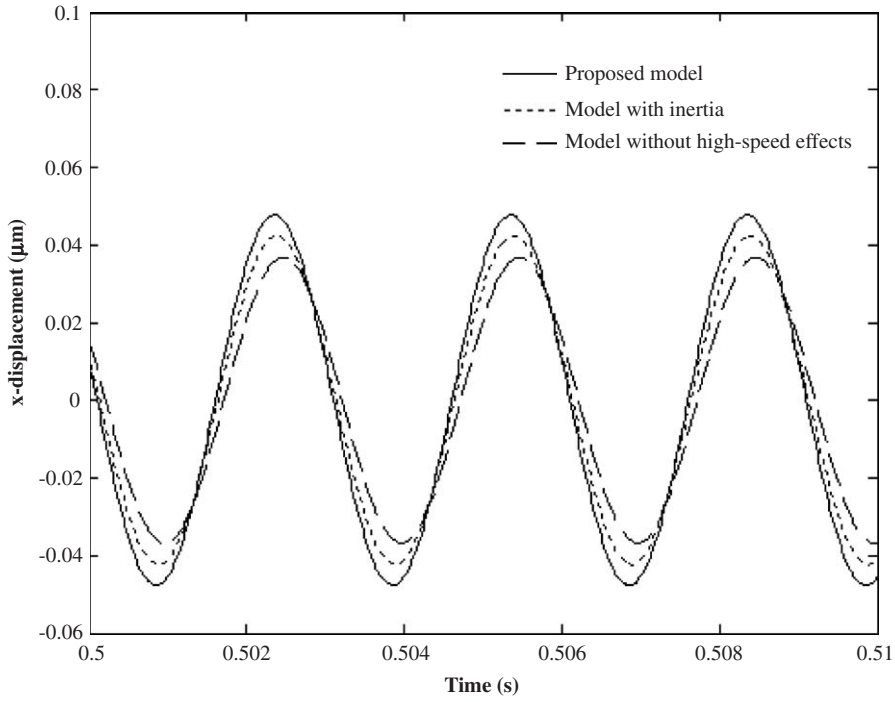

Fig. 6. Comparison of the x-displacement for three models, $P_z = 800$ N, $\omega = 2000$ rpm.

$$l_{ij} = \frac{L_{ij}\cos\alpha_0 + u_{rj} - v_{rj}}{\cos\alpha_{ij}} = \frac{L_{ij}\sin\alpha_0 + u_{zj} - v_{zj}}{\sin\alpha_{ij}}, \tag{20}$$

$$l_{oj} = \frac{L_{oj}\cos\alpha_0 + v_{rj}}{\cos\alpha_{oj}} = \frac{L_{oj}\sin\alpha_0 + v_{zj}}{\sin\alpha_{oj}}. \tag{21}$$

The contact deformation between the ball and race are as follows:

$$\delta_{ij} = l_{ij} - L_{ij} - c_i, \tag{22}$$

$$\delta_{oj} = l_{oj} - L_{oj} - c_o, \tag{23}$$

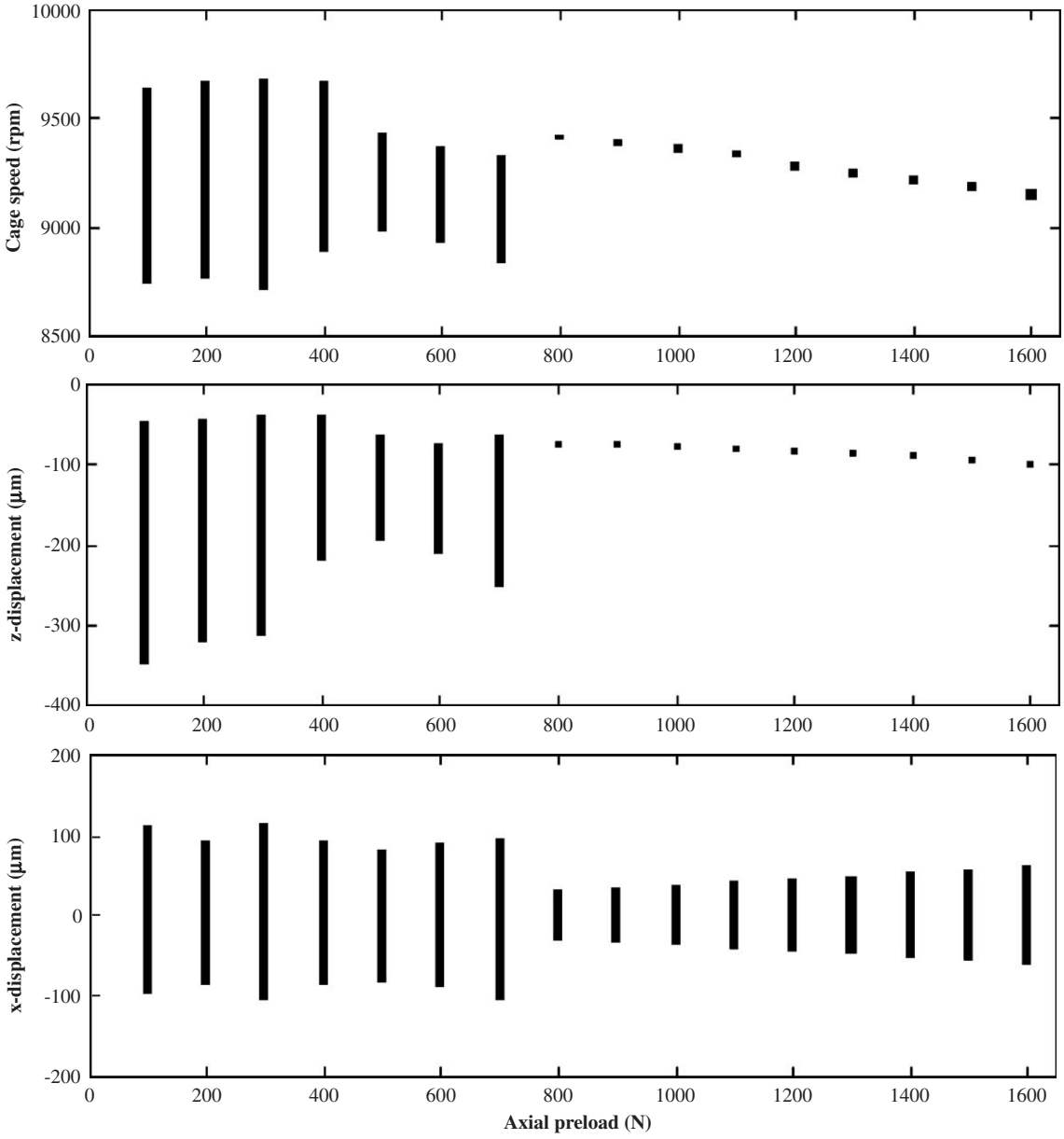

Fig. 7. Cage speed, z- and x-displacement variation on axial preload, $c_i = c_o = 4\text{e}{-}6\text{m}$, $\omega = 20\,000$ rpm.

where the negative values mean loss of contact. If the contact deformation is positive, the contact force could be calculated using the Hertzian contact theory; otherwise no load is transmitted. So the contact force can be expressed as

$$Q_{ij} = \chi_{ij} K_{ij} \delta_{ij}^{3/2}, \tag{24}$$

$$Q_{oj} = \chi_{oj} K_{oj} \delta_{oj}^{3/2}, \tag{25}$$

where

$$\chi_{ij} = \begin{cases} 1, & \delta_{ij} > 0, \\ 0, & \delta_{ij} \leqslant 0 \end{cases} \tag{26}$$

and

$$\chi_{oj} = \begin{cases} 1, & \delta_{oj} > 0, \\ 0, & \delta_{oj} \leqslant 0. \end{cases} \tag{27}$$

The load–deflection constants between the ball and each race, K_{ij} and K_{oj}, may be obtained using the simplified solution in Refs. [26,27] and are represented in Appendix A.

Fig. 4 shows the forces and moments acting on a ball in a high-speed ball bearing. The equilibrium of forces in the horizontal and vertical directions can thus be written with reference to Fig. 4.

$$\begin{Bmatrix} g_{rj} \\ g_{zj} \end{Bmatrix} = \begin{Bmatrix} Q_{ij}\cos\alpha_{ij} - Q_{oj}\cos\alpha_{oj} + \dfrac{\lambda_{ij}M_{gj}}{D_b}\sin\alpha_{ij} - \dfrac{\lambda_{oj}M_{gj}}{D_b}\sin\alpha_{oj} + F_{ej} \\ Q_{ij}\sin\alpha_{ij} - Q_{oj}\sin\alpha_{oj} - \dfrac{\lambda_{ij}M_{gj}}{D_b}\cos\alpha_{ij} + \dfrac{\lambda_{oj}M_{gj}}{D_b}\cos\alpha_{oj} \end{Bmatrix} = \begin{Bmatrix} 0 \\ 0 \end{Bmatrix}. \tag{28}$$

The centrifugal force and gyroscopic moment can be described as follows:

$$F_{ej} = \frac{D_p + 2v_{rj}}{2} m_{bj} \omega_{mj}^2, \tag{29}$$

$$M_{gj} = I_{bj} \omega_{bj} \omega_{mj} \sin\beta_j. \tag{30}$$

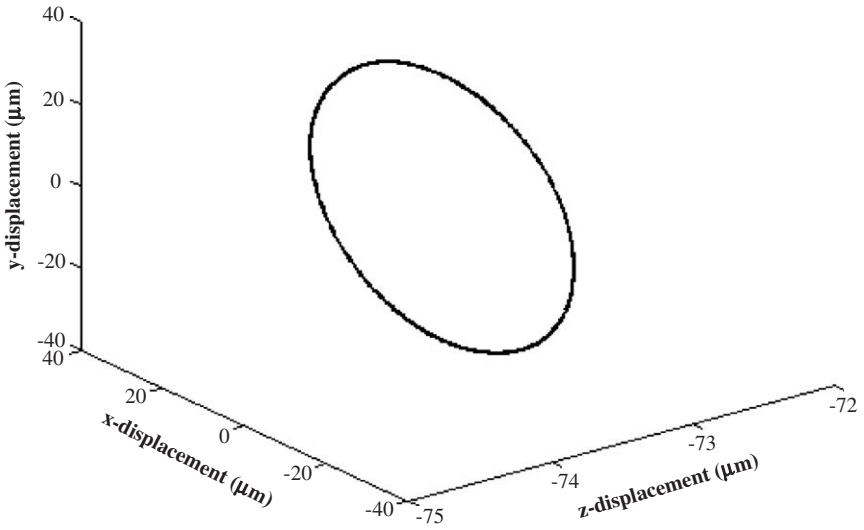

Fig. 8. Periodic orbit at $P_z = 800\,\mathrm{N}$.

It is assumed that the operating conditions of the ball bearing are so appropriate that the race control theory [3] is applicable. Then the unknown quantities in Eqs. (29), (30), β_j, ω_{bj} and ω_{mj}, could be conveniently determined and shown in Appendix B.

Eq. (28) is a set of nonlinear equations with two unknown ball center displacements v_{rj} and v_{zj}. For a given inner race position, $\{U\}$, the ball center displacements may be solved by applying the Newton–Raphson technique:

$$\begin{Bmatrix} v_{rj} \\ v_{zj} \end{Bmatrix}_{i+1} = \begin{Bmatrix} v_{rj} \\ v_{zj} \end{Bmatrix}_{i} - \begin{bmatrix} \dfrac{\partial g_{rj}}{\partial v_{rj}} & \dfrac{\partial g_{rj}}{\partial v_{zj}} \\ \dfrac{\partial g_{zj}}{\partial v_{rj}} & \dfrac{\partial g_{zj}}{\partial v_{zj}} \end{bmatrix}_{i}^{-1} \begin{Bmatrix} g_{rj} \\ g_{zj} \end{Bmatrix}_{i}. \tag{31}$$

The Jacobian matrix is explained in more detail in Appendix C.

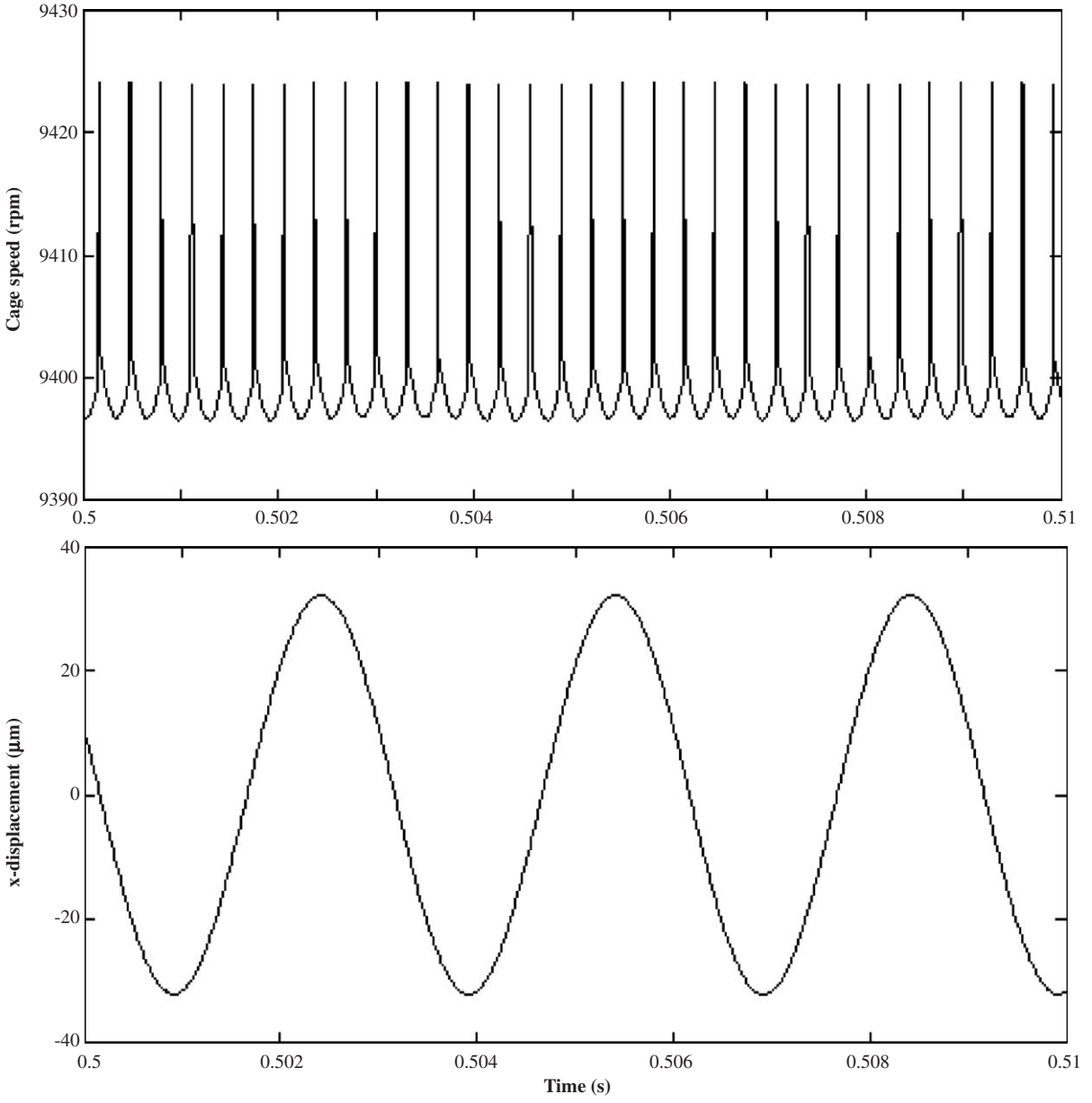

Fig. 9. Time-domain responses for cage speed and x-displacement at $P_z = 800\,\mathrm{N}$.

2.4. Contact forces and equations of motion

So the contact forces for the jth rolling element in the local rolling element coordinate system are written as

$$\{Q_j\} = \begin{Bmatrix} Q_{rj} \\ Q_{zj} \\ Q_{\phi j} \end{Bmatrix} = \begin{Bmatrix} -Q_{ij}\cos\alpha_{ij} - \dfrac{\lambda_{ij}M_{gj}}{D_b}\sin\alpha_{ij} \\ -Q_{ij}\sin\alpha_{ij} + \dfrac{\lambda_{ij}M_{gj}}{D_b}\sin\alpha_{ij} \\ -\dfrac{\lambda_{ij}M_{gj}}{D_b}r_i \end{Bmatrix}. \tag{32}$$

The contact force vector for each rolling element can be transformed to an equivalent force vector in the inertial coordinate system using the transformation matrix, $[T_j]$. Therefore summing the equivalent vectors for all rolling elements, the total bearing force vector is obtained from

$$\{F\} = \{F_x \quad F_y \quad F_z \quad M_x \quad M_y\}^{\mathrm{T}} = \sum_{j=1}^{N} [T_j]^{\mathrm{T}}\{Q_j\}. \tag{33}$$

The equations of motion for a rotor bearing system may be written as

$$[m]\{\ddot{X}\} + [d]\{\dot{X}\} + [k]\{X\} = \{f(X,t)\}, \tag{34}$$

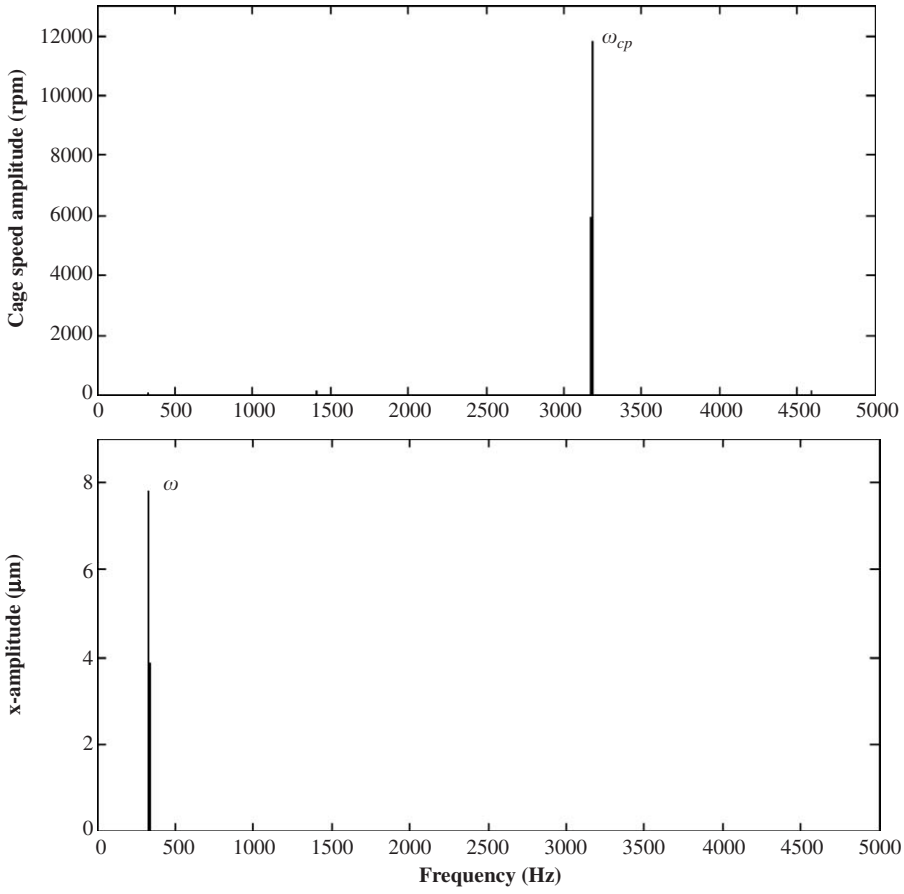

Fig. 10. Power spectra of cage speed and x-displacement at $P_z = 800\,\mathrm{N}$.

where the force vector $\{f\}$ could include the total nonlinear bearing forces, external load, gravity load and unbalance load.

For a 5dof system, the equations of motion can be represented as follows:

$$\begin{aligned} m\ddot{x} &= F_x + P_x + me\omega^2 \cos \omega t, \\ m\ddot{y} &= F_y + P_y + me\omega^2 \sin \omega t, \\ m\ddot{z} &= F_z + P, \\ I_r\ddot{\theta}_x + I_z\omega\dot{\theta}_y &= M_x, \\ I_r\ddot{\theta}_y - I_z\omega\dot{\theta}_x &= M_y, \end{aligned} \tag{35}$$

where $me\omega^2$ indicates the unbalance load due to the rotor mass eccentricity e.

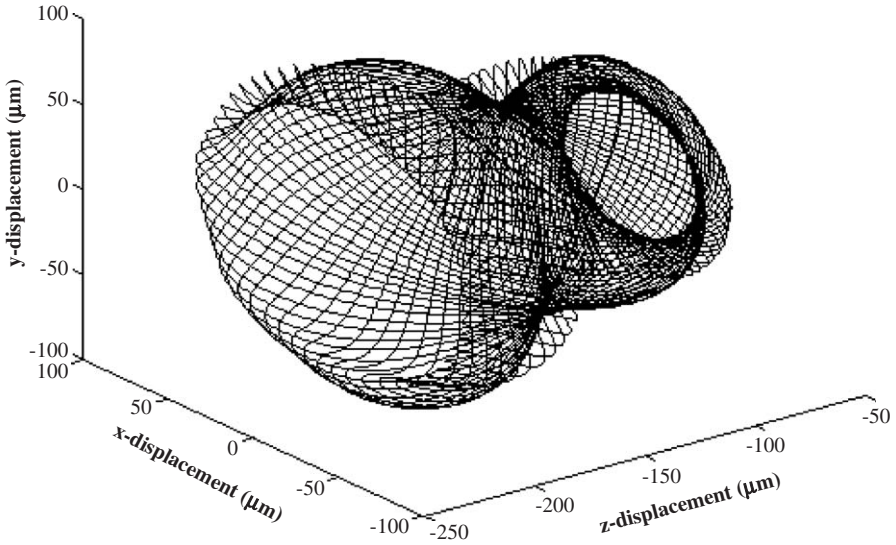

Fig. 11. Quasi-periodic orbit at $P_z = 600\,\mathrm{N}$.

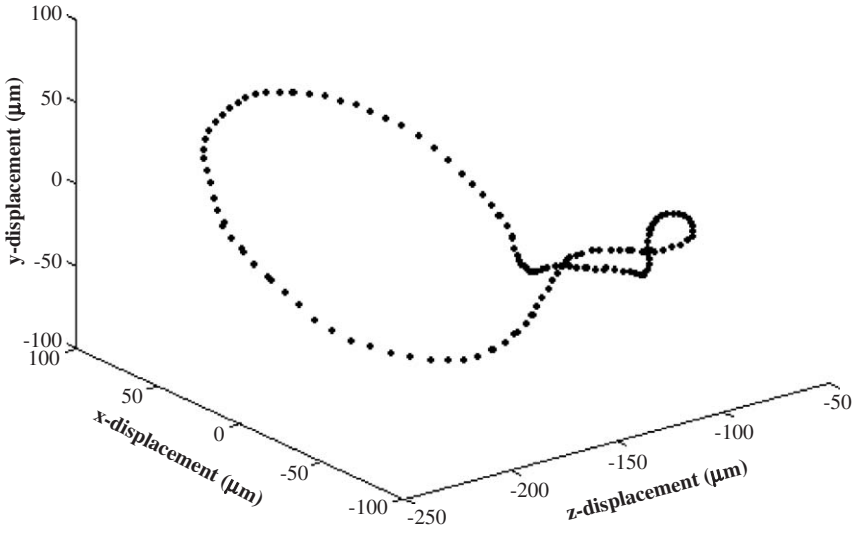

Fig. 12. Poincarè map at $P_z = 600\,\mathrm{N}$.

Using the Newmark-β method, the differential equations of motion can be solved and the transient responses at every time increment are obtained. Note that the iterations at every time increment should be applied to achieving an adequate accuracy.

3. Results and discussion

3.1. Validation of the ball bearing model

The applicability of the ball bearing model to reality can be demonstrated by experiment. Table 1 shows the dimensions of the ball bearing used by Gupta [28]. According to the bearing geometry reported in Ref. [28], the approximate mass of the rotor bearing system is $m = 12.17\,\mathrm{kg}$ and the radial and polar mass moment of inertia are $I_r = 0.0330\,\mathrm{kg\,m^2}$ and $I_z = 0.0609\,\mathrm{kg\,m^2}$, respectively. Then the rotor bearing system can be modeled by the differential equations of motion, Eq. (35).

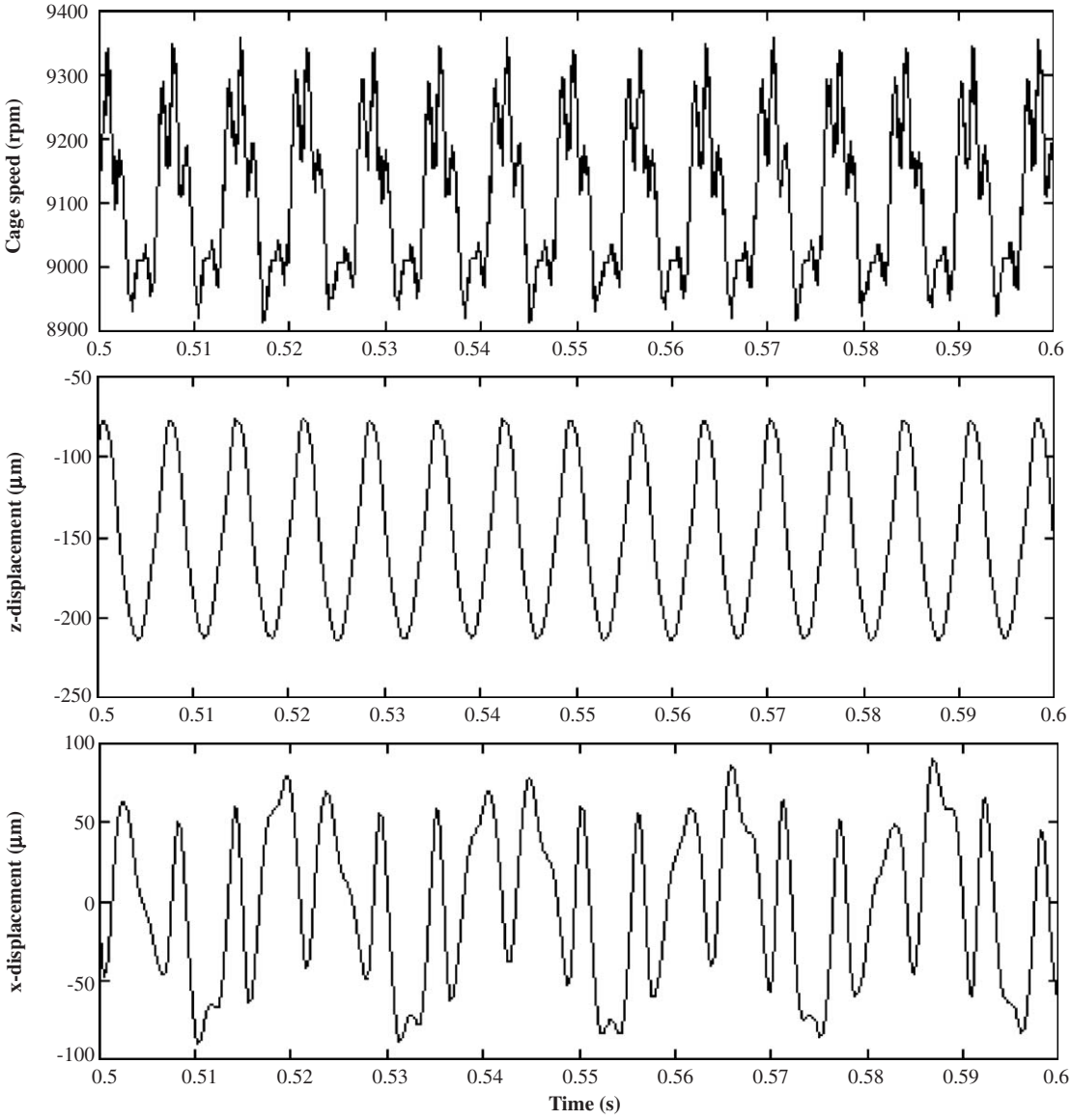

Fig. 13. Time domain responses for cage speed, z- and x-displacement at $P_z = 600\,\mathrm{N}$.

Let the rotor mass eccentricity e be 2e−5m. At the shaft speed $\omega = 2500,5000,10\,000$, and $20\,000$ rpm, respectively, the variation of the cage speed is calculated and depicted in Fig. 5, where the experimental data and Gupta analysis [28] are also described. It shows that the results obtained from the proposed model are in good agreement with the test data and more reasonable than Gupta analysis, especially at high speed.

With the theoretical verification the ball bearing model can be checked if the mathematical model gives results which are equivalent to other mathematical models. In low-speed operation, the centrifugal force and gyroscopic moment from balls exert slight effects, and then the proposed model can be compared with two already existing models, 5dof model without considering high-speed effects and 5dof model only with ball centrifugal force. Fig. 6 shows the comparison of x-displacement for three models at low speed $\omega = 2000$ rpm. Clearly, these three solutions are closely similar. Note that the better agreement with the proposed analysis is achieved when the ball centrifugal force is taken into account. Thus, the small differences between the three curves in Fig. 6 can be attributed to the effects of centrifugal force and gyroscopic moment from balls.

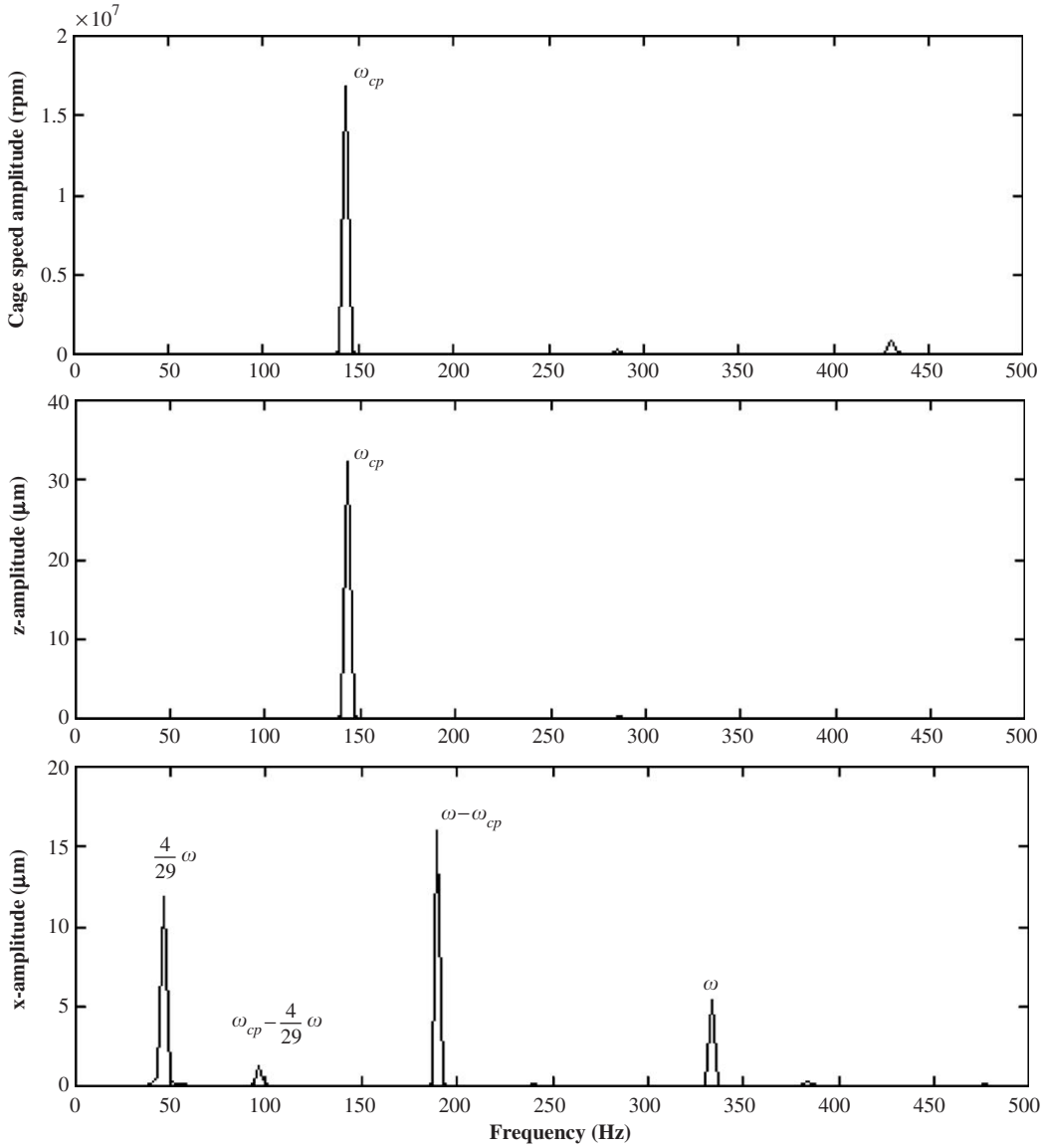

Fig. 14. Power spectra of cage speed, z- and x-displacement at $P_z = 600$ N.

3.2. Effect of the axial preload

The cage speed, z- and x-displacement variation on axial preload are shown in Fig. 7 when $c_i = c_o = 4e{-}6m$, $e = 1e{-}5m$ and $\omega = 20\,000$ rpm. It can be found that the peak-to-peak amplitude of cage speed rises markedly when the axial preload is less than 800 N. The changes in z- and x-displacement are similar to that in cage speed. It means that the periodic solution loses stability according to the discussion in the following, and the system stability can be determined with the aid of the Floquet theory [29].

Fig. 8 depicts the three-dimensional period orbit when the axial preload is $P_z = 800$ N and $c_i = c_o = 4e{-}6m$, $e = 1e - 5m$. Stability analysis shows that the leading Floquet multipliers are $-7.7911 \pm 2.5389i$ and the absolute value of the leading Floquet multipliers is 0.8194, less than one, which indicates that the periodic solution of the system is stable in the Liapunov sense. The time domain responses of the period motion for cage speed and x-displacement are shown in Fig. 9 and the corresponding power spectra are plotted in Fig. 10, where ω_{cp} represents the principal frequency of cage speed. As the response is stable periodic solution, ω_{cp} approximates to the ball passage frequency [7], which has been defined as the arithmetic product of the number of balls and the cage speed that is assumed as a fixed constant. Referring to the power spectra of the displacement in x-direction in Fig. 10, the resonant frequency, equal to shaft frequency ω, indicates the response is a period-1 motion.

At $P_z = 600$ N, the leading Floquet multipliers are $-1.2041 \pm 1.4228i$ and the absolute value of the leading Floquet multipliers is 1.8639. This shows that a pair of complex–conjugate Floquet multipliers leaves the unit circle in the complex plane, which indicates that the periodic response loses stability and undergoes a

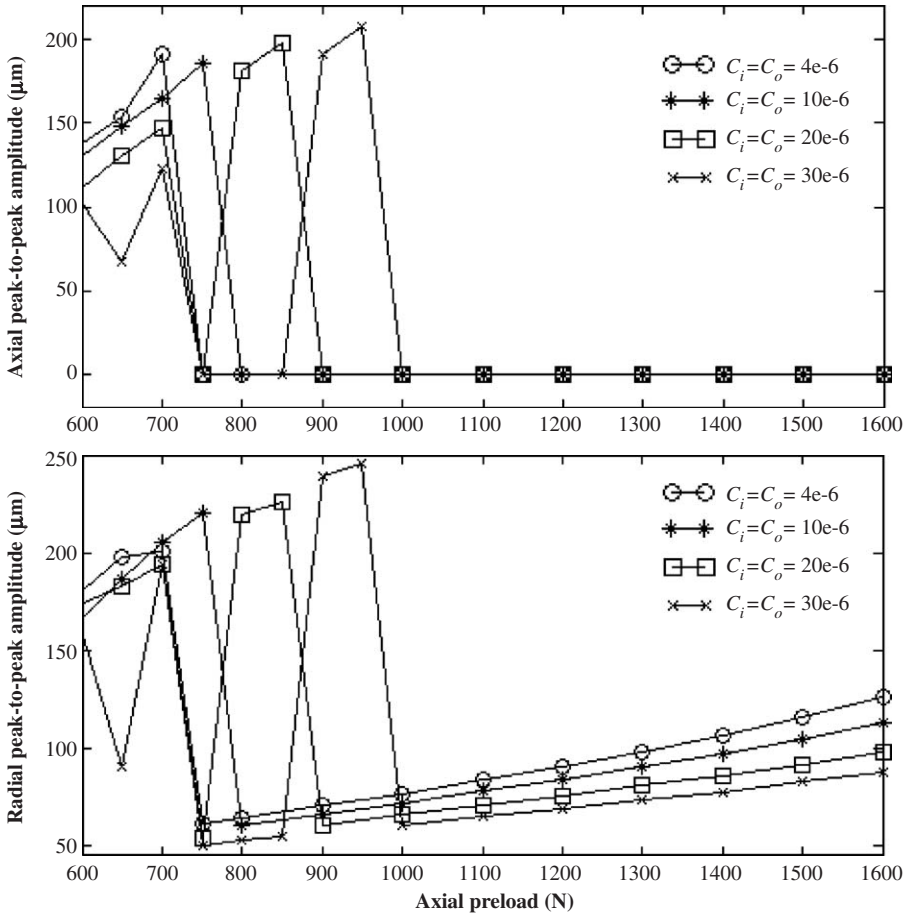

Fig. 15. Effect of clearance variation on axial and radial peak-to-peak amplitudes as a function of axial preload, $\omega = 20\,000$ rpm.

secondary Hopf bifurcation to a quasi-periodic motion. The quasi-periodic orbit is depicted in Fig. 11. It is shown that not only the radial amplitude but also the axial amplitude has a dramatic increase. By Poincarè map plotted in Fig. 12 shows a closed curve which indicates that the response is a quasi-periodic motion. Comparing Fig. 13 with Fig. 9, it can be seen that the time history for cage speed and x-displacement become complicated and the peak-to-peak amplitudes rise significantly. Moreover, the principal frequency of the cage speed, which is just the resonant frequency of z-displacement, is far less than the ball passage frequency (Fig. 14). Referring to the power spectra of the z- and x-displacement in Fig. 14, all the frequency peaks are some combinations of two basic components ω and ω_{cp}, but independent of the ball passage frequency.

3.3. Effect of the clearance

In order to investigate the vibration characteristics under the effect of the clearance, the axial and radial peak-to-peak amplitudes are analyzed in the axial preload interval $P_z = 600$ to 1600 N for four values of clearance $c_i = c_o = 4\text{e}{-}6\text{m}$, $10\text{e}{-}6\text{m}$, $20\text{e}{-}6\text{m}$ and $30\text{e}{-}6\text{m}$. The results are described in Fig. 15 where the dramatic increase of peak-to-peak amplitude implies the periodic solution becomes unstable according to the stability analysis. It is clearly shown that the critical axial preload where the periodic solution loses stable increases with an increase in clearance value. Moreover, the other stable interval occurs near $P_z = 750\,\text{N}$ when $c_i = c_o = 20\text{e}{-}6\text{m}$ and increases as clearance increases. Fig. 15 is shown that the new stable interval expands from near $P_z = 750\,\text{N}$ at $c_i = c_o = 20\text{e}{-}6\text{m}$ to between $P_z = 750$ and 850 N at $c_i = c_o = 30\text{e}{-}6\text{m}$. In the axial preload interval of stable periodic solution, the radial peak-to-peak amplitude increases as the axial preload increases and decreases as the clearance rises. It interesting that the axial peak-to-peak amplitude remains unchanged in the stable axial preload interval. Furthermore, Fig. 16 shows the effect of clearance variation on maximum cage speed as a function of axial preload. The maximum cage speed decreases with an increase in axial preload and clearance when the system response is stable.

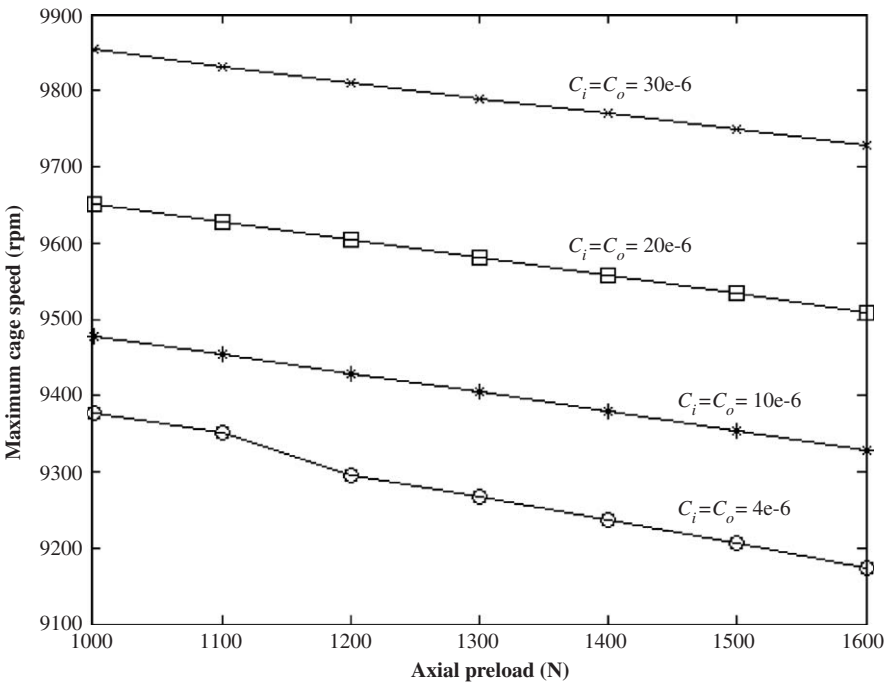

Fig. 16. Effect of clearance variation on maximum cage speed as a function of axial preload, $\omega = 20\,000$ rpm.

3.4. Effect of the radial load

Fig. 17 plots the z-displacement variation on axial preload under the effect of the radial load. The critical axial preload where the system response becomes unstable changes from 1350 to 1150 N when the radial load is from $P_x = P_y = 500$ N to $P_x = P_y = 200$ N. Moreover, the critical axial preload is 650 N at $P_x = P_y = 0$, as Fig. 7 shows. It indicates that the critical axial preload decreases as radial load falls. Otherwise an increase in clearance leads to an increase in critical axial preload and a decrease in axial peak-to-peak amplitude.

Figs. 18 and 19 depict the frequency response when the radial load is taken into account. When $P_x = P_y = 200$ N and $P_z = 1200$ N, the periodic motion is stable and the power spectra of cage speed and x-displacement are plotted in Fig. 18. Note that the principal frequency of cage speed ω_{cp} approximates not to the ball passage frequency (Fig. 10), but to the resonant frequency of the radial motion, ω due to the

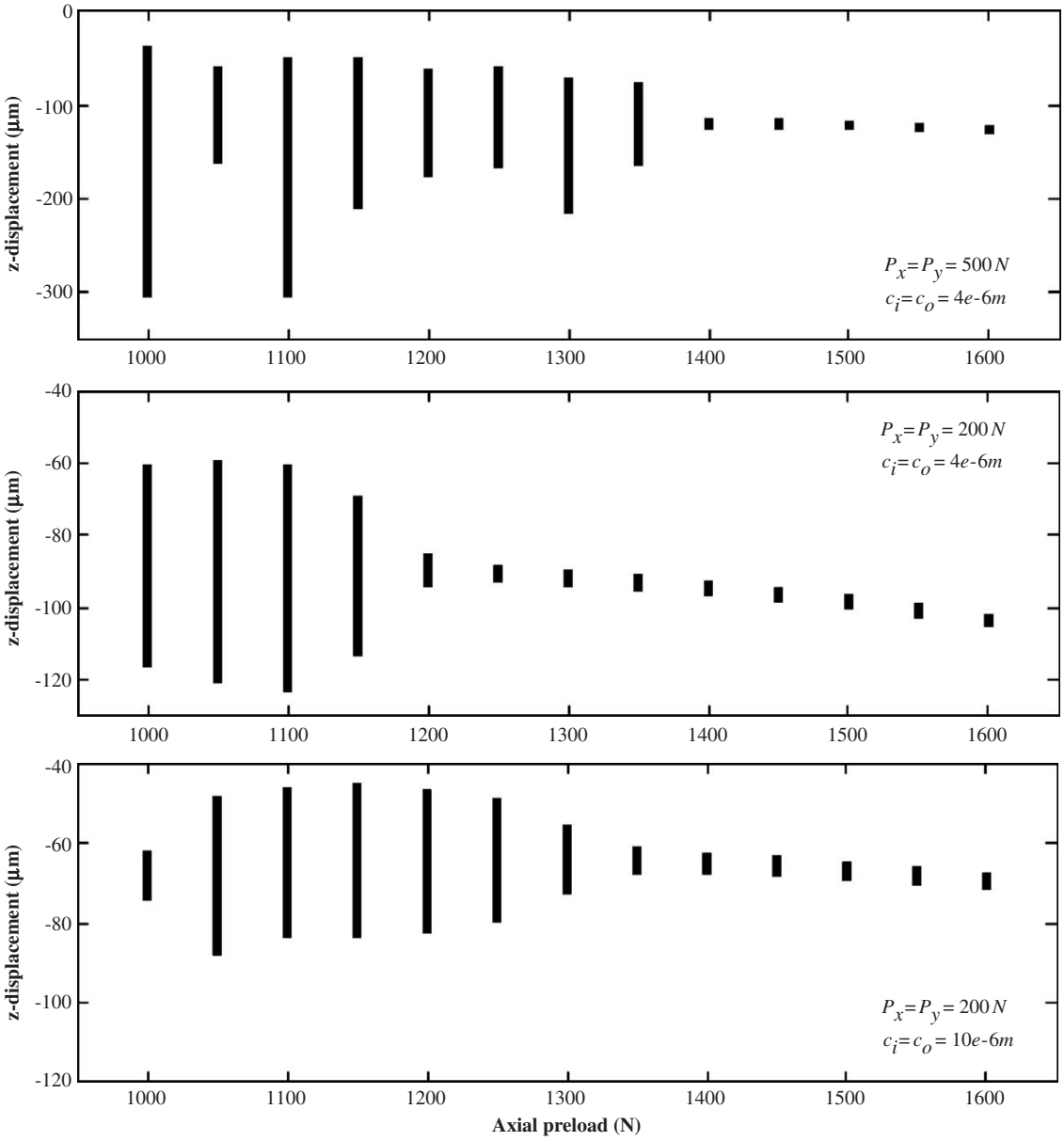

Fig. 17. Effects of radial load and clearance variation on z-displacement as a function of axial preload, $\omega = 20\,000$ rpm.

contribution of radial load. Fig. 19 shows some combinations of the two basic frequencies ω and ω_{cp} when the response is a quasi-periodic motion at $P_x = P_y = 200\,\mathrm{N}$ and $P_z = 1100\,\mathrm{N}$. It is shown that the power spectra of cage speed are more complex than that shown in Fig. 14 and ω_{cp} drops significantly when the radial load is applied.

3.5. Effect of the waviness

Fig. 20 describes the effect of waviness on the time history of cage speed. The inner race and outer race have the wariness of order 18 and amplitude 1e−6m. The ball has waviness of order 2 and amplitude 1e−6m. Due to the high-speed effect of ball centrifugal force and gyroscopic moment, the cage speed variation under the effect of outer race waviness is more considerable than that under the effect of inner race and ball waviness. Moreover, the effect of ball waviness on cage speed variation is unapparent.

4. Conclusion

A 5dof transient dynamic model of ball bearings is presented to investigate the dynamic stability and vibration characteristics of rotor bearing system. The effects of both the clearance between the balls and races and the waviness on bearing running surface are taken into account. Further, the model includes the high-speed effects of the ball centrifugal force and gyroscopic moment. The cage speed is determined by the orbital speed of balls. The results obtained from the proposed model are in good agreement with prior authors' test data and already existing models. It is shown that the proposed analysis is more reasonable than their numeric analysis, especially at high speed.

From the investigations of the nonlinear stability and dynamic properties of a rigid rotor supported by a ball bearing, the following conclusions can be drawn:

- When the axial preload is less than the critical value, the periodic solution loses stability and the peak-to-peak amplitudes of cage speed and axial and radial displacement have a dramatic increase.

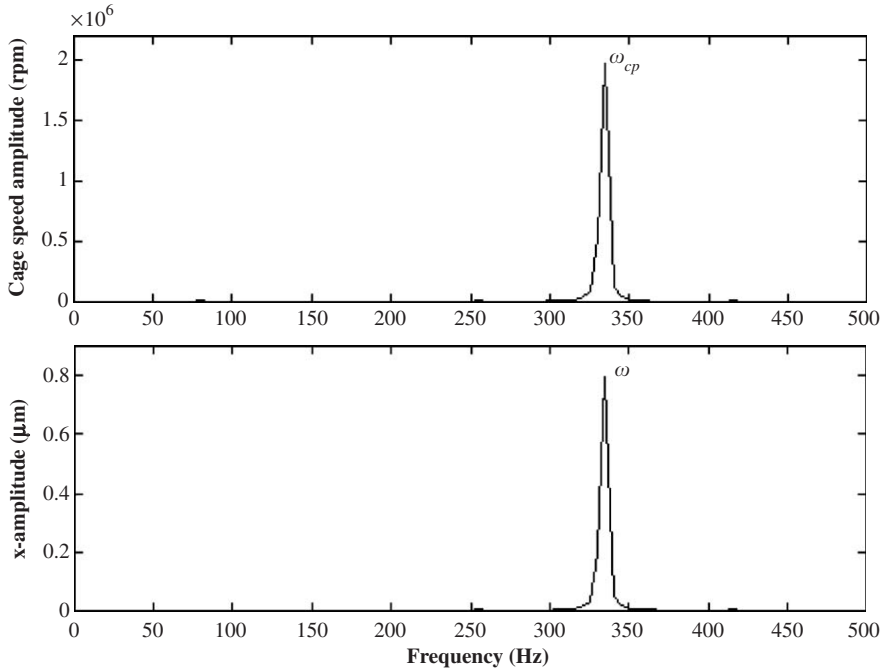

Fig. 18. Power spectra of cage speed and x-displacement, $P_x = P_y = 200\,\mathrm{N}$, $P_z = 1200\,\mathrm{N}$, $c_i = c_o = 4\mathrm{e}{-6}\mathrm{m}$.

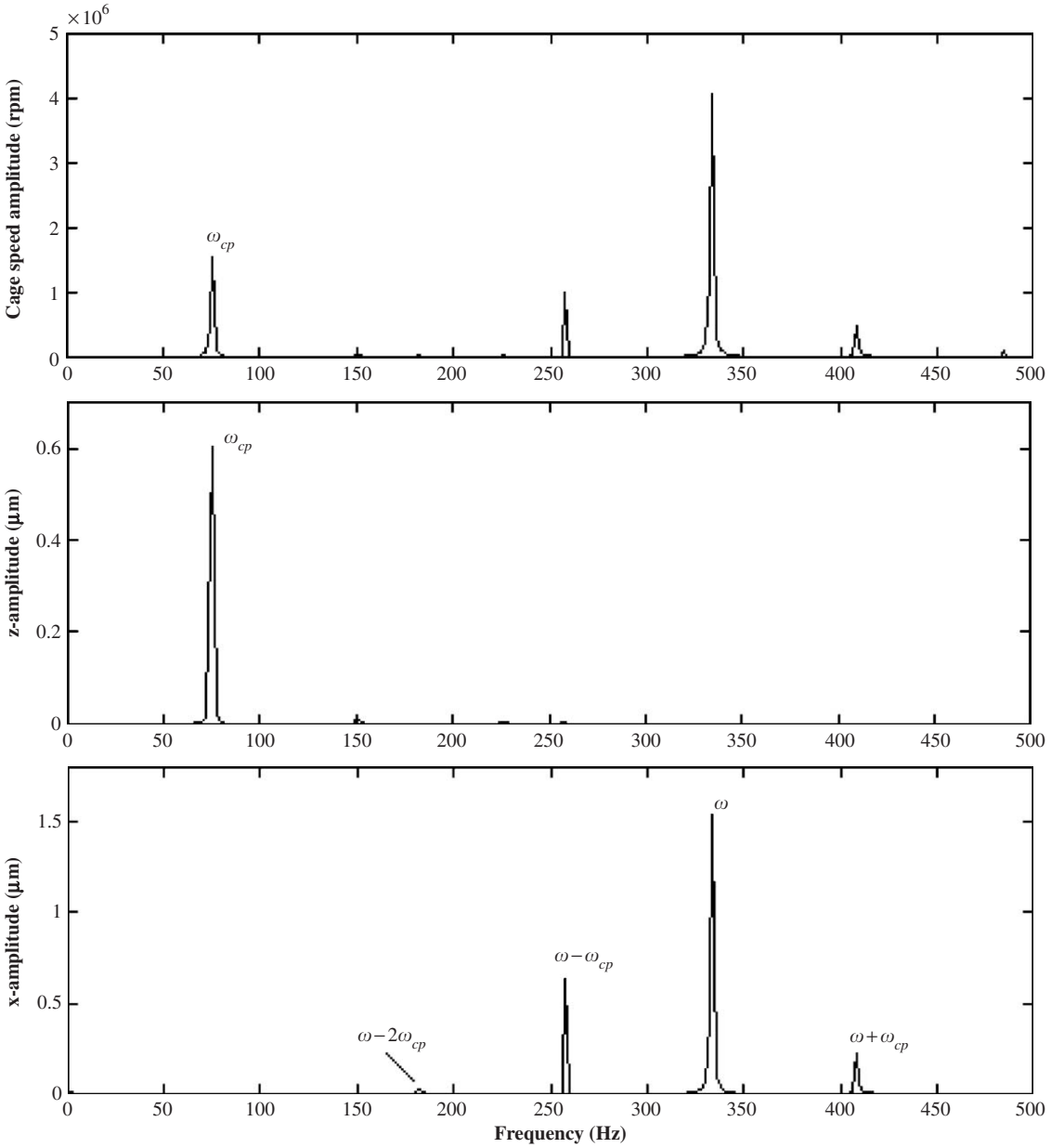

Fig. 19. Power spectra of cage speed, z- and x-displacement, $P_x = P_y = 200\,\mathrm{N}$, $P_z = 1100\,\mathrm{N}$, $c_i = c_o = 4\mathrm{e}{-6}\mathrm{m}$.

- The principal frequency of cage speed is a basic component of system vibration frequencies. It could be far less than the ball passage frequency as the system response is unstable or the radial load exists.
- Effect of clearance on system stability is significant. The critical axial preload where the periodic solution loses stability increases with an increase in clearance value. In the axial preload interval of stable periodic solution, the radial peak-to-peak amplitude decreases and the axial peak-to-peak amplitude remains unchanged as the clearance rises. Furthermore, the maximum cage speed decreases with an increase in axial preload and clearance.
- The critical axial preload increases with radial load.

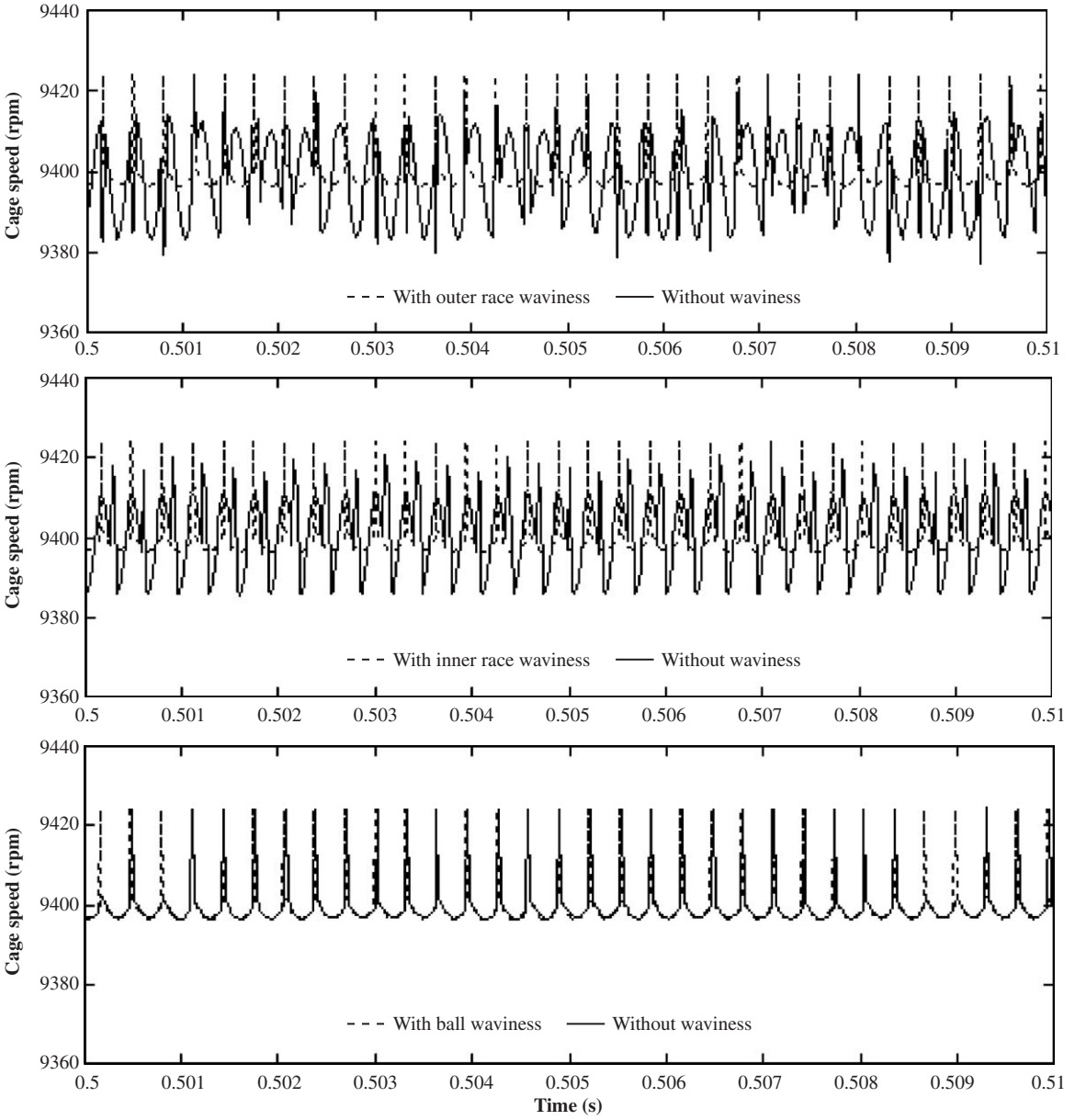

Fig. 20. Effect of waviness on cage speed, $P_z = 800\,\mathrm{N}$, $c_i = c_o = 4\mathrm{e}{-6}\mathrm{m}$, $\omega = 20\,000\,\mathrm{rpm}$.

- The effect of ball waviness on cage speed variation is unapparent and the effect of outer race waviness is more considerable than that of inner race and ball waviness.

Acknowledgment

The authors would like to acknowledge the support of the Doctoral Dissertation Foundation of Xi'an Jiaotong University (DFXJTU 2003-9). This work was also partially supported by the National Natural Science Foundation of China (50275113) and the Doctoral Science Foundation of Ministry of Education (20030698017).

Appendix A. Load-deflection constants

The classical Hertzian solution can be simplified using a linear regression by the method of least squares. The load–deflection constants between the ball and each race, K_{ij} and K_{oj}, can be expressed as

$$K_{ij} = \frac{\pi E}{1-v^2}\,\bar{k}_{ij}\left(\frac{\bar{R}_{ij}\bar{E}_{ij}}{4.5\bar{F}_{ij}^3}\right)^{1/2}, \quad K_{oj} = \frac{\pi E}{1-v^2}\,\bar{k}_{oj}\left(\frac{\bar{R}_{oj}\bar{E}_{oj}}{4.5\bar{F}_{oj}^3}\right)^{1/2}, \tag{A.1}$$

where E and v are the Young's modulus and by Poisson ratio of contact material and $\bar{k}$, $\bar{E}$ and $\bar{F}$ can be expressed, respectively, as follows:

$$\bar{k}_{ij} = 1.0339(R_{yij}/R_{xij})^{0.6360}, \quad \bar{k}_{oj} = 1.0339(R_{yoj}/R_{xoj})^{0.6360}, \tag{A.2}$$

$$\bar{E}_{ij} = 1.0003 + \frac{0.5968}{R_{yij}/R_{xij}}, \quad \bar{E}_{oj} = 1.0003 + \frac{0.5968}{R_{yoj}/R_{xoj}}, \tag{A.3}$$

$$\bar{F}_{ij} = 1.5277 + 0.6023\ln(R_{yij}/R_{xij}), \quad \bar{F}_{oj} = 1.5277 + 0.6023\ln(R_{yoj}/R_{xoj}), \tag{A.4}$$

$$\bar{R}_{ij} = \frac{R_{xij}R_{yij}}{R_{xij}+R_{yij}}, \quad \bar{R}_{oj} = \frac{R_{xoj}R_{yoj}}{R_{xoj}+R_{yoj}}. \tag{A.5}$$

The effective radius can be written for the ball–inner-race contact as

$$R_{xij} = \frac{D_b(D_p - D_b\cos\alpha_{ij})}{2D_p}, \quad R_{yij} = \frac{r_i}{2r_i/D_b - 1}. \tag{A.6}$$

and for the ball–outer-race contact as

$$R_{xoj} = \frac{D_b(D_p + D_b\cos\alpha_{oj})}{2D_p}, \quad R_{yoj} = \frac{r_o}{2r_o/D_b - 1}. \tag{A.7}$$

Appendix B. Angle between ball rotational axis and bearing centerline and the angular velocity of ball and ball orbital

According to the race control theory, the angle between the ball rotational axis and the bearing centerline β_j, the angular velocity of ball ω_{bj} and angular velocity ball orbital ω_{mj} can be determined and shown as

Inner race control:

$$\lambda_{ij} = 1, \quad \lambda_{oj} = 1, \tag{B.1}$$

$$\tan\beta_j = \frac{\sin\alpha_{ij}}{\cos\alpha_{ij} - \gamma}, \tag{B.2}$$

$$\omega_{bj} = -\omega_i\frac{(\cos\alpha_{ij} - \gamma)(1 + \gamma\cos\alpha_{oj})}{\gamma[1 + \cos(\alpha_{ij} - \alpha_{oj})]\cos\beta_j}, \tag{B.3}$$

$$\omega_{mj} = \omega_i\frac{\cos(\alpha_{ij} - \alpha_{oj}) - \gamma\cos\alpha_{oj}}{1 + \cos(\alpha_{ij} - \alpha_{oj})}. \tag{B.4}$$

Outer race control:

$$\lambda_{ij} = 0, \quad \lambda_{oj} = 2, \tag{B.5}$$

$$\tan\beta_j = \frac{\sin\alpha_{oj}}{\cos\alpha_{oj} + \gamma}, \tag{B.6}$$

$$\omega_{bj} = -\omega_i \frac{(\cos\alpha_{oj} + \gamma)(1 - \gamma\cos\alpha_{ij})}{\gamma[1 + \cos(\alpha_{ij} - \alpha_{oj})]\cos\beta_j}, \tag{B.7}$$

$$\omega_{mj} = \omega_i \frac{1 - \gamma\cos\alpha_{ij}}{1 + \cos(\alpha_{ij} - \alpha_{oj})}. \tag{B.8}$$

Appendix C. Components of Jacobian matrix

The equilibrium Jacobian matrix is needed in Eq. (31) to solve the ball displacement. The partial derivatives with respect to the displacement of jth ball center can be given by

$$\begin{aligned}\frac{\partial g_{rj}}{\partial v_{rj}} = {} & \cos\alpha_{ij}\frac{\partial Q_{ij}}{\partial v_{rj}} - Q_{ij}\sin\alpha_{ij}\frac{\partial \alpha_{ij}}{\partial v_{rj}} - \cos\alpha_{oj}\frac{\partial Q_{oj}}{\partial v_{rj}} + Q_{oj}\sin\alpha_{oj}\frac{\partial \alpha_{oj}}{\partial v_{rj}} \\ & + \frac{\lambda_{ij}\sin\alpha_{ij} - \lambda_{oj}\sin\alpha_{oj}}{D_b}\frac{\partial M_{gj}}{\partial v_{rj}} + \frac{\lambda_{ij}M_{gj}\cos\alpha_{ij}}{D_b}\frac{\partial \alpha_{ij}}{\partial v_{rj}} - \frac{\lambda_{oj}M_{gj}\cos\alpha_{oj}}{D_b}\frac{\partial \alpha_{oj}}{\partial v_{rj}} + \frac{\partial F_{ej}}{\partial v_{rj}},\end{aligned} \tag{C.1}$$

$$\begin{aligned}\frac{\partial g_{rj}}{\partial v_{zj}} = {} & \cos\alpha_{ij}\frac{\partial Q_{ij}}{\partial v_{zj}} - Q_{ij}\sin\alpha_{ij}\frac{\partial \alpha_{ij}}{\partial v_{zj}} - \cos\alpha_{oj}\frac{\partial Q_{oj}}{\partial v_{zj}} + Q_{oj}\sin\alpha_{oj}\frac{\partial \alpha_{oj}}{\partial v_{zj}} \\ & + \frac{\lambda_{ij}\sin\alpha_{ij} - \lambda_{oj}\sin\alpha_{oj}}{D_b}\frac{\partial M_{gj}}{\partial v_{zj}} + \frac{\lambda_{ij}M_{gj}\cos\alpha_{ij}}{D_b}\frac{\partial \alpha_{ij}}{\partial v_{zj}} - \frac{\lambda_{oj}M_{gj}\cos\alpha_{oj}}{D_b}\frac{\partial \alpha_{oj}}{\partial v_{zj}} + \frac{\partial F_{ej}}{\partial v_{zj}},\end{aligned} \tag{C.2}$$

$$\begin{aligned}\frac{\partial g_{zj}}{\partial v_{rj}} = {} & \sin\alpha_{ij}\frac{\partial Q_{ij}}{\partial v_{rj}} + Q_{ij}\cos\alpha_{ij}\frac{\partial \alpha_{ij}}{\partial v_{rj}} - \sin\alpha_{oj}\frac{\partial Q_{oj}}{\partial v_{rj}} - Q_{oj}\cos\alpha_{oj}\frac{\partial \alpha_{oj}}{\partial v_{rj}} \\ & - \frac{\lambda_{ij}\cos\alpha_{ij} - \lambda_{oj}\cos\alpha_{oj}}{D_b}\frac{\partial M_{gj}}{\partial v_{rj}} + \frac{\lambda_{ij}M_{gj}\sin\alpha_{ij}}{D_b}\frac{\partial \alpha_{ij}}{\partial v_{rj}} - \frac{\lambda_{oj}M_{gj}\sin\alpha_{oj}}{D_b}\frac{\partial \alpha_{oj}}{\partial v_{rj}},\end{aligned} \tag{C.3}$$

$$\begin{aligned}\frac{\partial g_{zj}}{\partial v_{zj}} = {} & \sin\alpha_{ij}\frac{\partial Q_{ij}}{\partial v_{zj}} + Q_{ij}\cos\alpha_{ij}\frac{\partial \alpha_{ij}}{\partial v_{zj}} - \sin\alpha_{oj}\frac{\partial Q_{oj}}{\partial v_{zj}} - Q_{oj}\cos\alpha_{oj}\frac{\partial \alpha_{oj}}{\partial v_{zj}} \\ & - \frac{\lambda_{ij}\cos\alpha_{ij} - \lambda_{oj}\cos\alpha_{oj}}{D_b}\frac{\partial M_{gj}}{\partial v_{zj}} + \frac{\lambda_{ij}M_{gj}\sin\alpha_{ij}}{D_b}\frac{\partial \alpha_{ij}}{\partial v_{zj}} - \frac{\lambda_{oj}M_{gj}\sin\alpha_{oj}}{D_b}\frac{\partial \alpha_{oj}}{\partial v_{zj}},\end{aligned} \tag{C.4}$$

where

$$\frac{\partial \alpha_{ij}}{\partial v_{rj}} = \frac{\sin\alpha_{ij}}{l_{ij}}, \quad \frac{\partial \alpha_{oj}}{\partial v_{rj}} = -\frac{\sin\alpha_{oj}}{l_{oj}}, \tag{C.5}$$

$$\frac{\partial \alpha_{ij}}{\partial v_{zj}} = -\frac{\cos\alpha_{ij}}{l_{ij}}, \quad \frac{\partial \alpha_{oj}}{\partial v_{zj}} = \frac{\cos\alpha_{oj}}{l_{oj}}, \tag{C.6}$$

and

$$\frac{\partial Q_{ij}}{\partial v_{rj}} = \chi_{ij}\delta_{ij}^{3/2}\frac{\partial K_{ij}}{\partial v_{rj}} - 1.5\chi_{ij}K_{ij}\delta_{ij}^{1/2}\cos\alpha_{ij}, \tag{C.7}$$

$$\frac{\partial Q_{oj}}{\partial v_{rj}} = \chi_{oj}\delta_{oj}^{3/2}\frac{\partial K_{oj}}{\partial v_{rj}} + 1.5\chi_{oj}K_{oj}\delta_{oj}^{1/2}\cos\alpha_{oj}, \tag{C.8}$$

$$\frac{\partial Q_{ij}}{\partial v_{zj}} = \chi_{ij}\delta_{ij}^{3/2}\frac{\partial K_{ij}}{\partial v_{zj}} - 1.5\chi_{ij}K_{ij}\delta_{ij}^{1/2}\sin\alpha_{ij}, \tag{C.9}$$

$$\frac{\partial Q_{oj}}{\partial v_{zj}} = \chi_{oj}\delta_{oj}^{3/2}\frac{\partial K_{oj}}{\partial v_{zj}} + 1.5\chi_{oj}K_{oj}\delta_{oj}^{1/2}\sin\alpha_{oj}. \tag{C.10}$$

$\partial K_{ij}/\partial v_{rj}$ and $\partial K_{ij}/\partial v_{rj}$ can be expressed as a uniform form $\partial K_{ij}/\partial v$, in which v denotes v_r or v_z; then

$$\frac{\partial K_{ij}}{\partial v} = \frac{\pi E}{1-\nu^2}\left(\frac{\bar{R}_{ij}\bar{E}_{ij}}{4.5\bar{F}_{ij}^3}\right)^{1/2}\left[\frac{\partial \bar{k}_{ij}}{\partial v} + \frac{\bar{k}_{ij}}{2\bar{R}_{ij}\bar{E}_{ij}\bar{F}_{ij}}\left(\bar{E}_{ij}\bar{F}_{ij}\frac{\partial \bar{R}_{ij}}{\partial v} + \bar{R}_{ij}\bar{F}_{ij}\frac{\partial \bar{E}_{ij}}{\partial v} - 3\bar{R}_{ij}\bar{E}_{ij}\frac{\partial \bar{F}_{ij}}{\partial v}\right)\right], \tag{C.11}$$

$$\frac{\partial \bar{k}_{ij}}{\partial v} = 0.6576(R_{yij}/R_{xij})^{-0.3640}\frac{\partial (R_{yij}/R_{xij})}{\partial v}, \tag{C.12}$$

$$\frac{\partial \bar{E}_{ij}}{\partial v} = -\frac{0.5968}{(R_{yij}/R_{xij})^2}\frac{\partial (R_{yij}/R_{xij})}{\partial v}, \tag{C.13}$$

$$\frac{\partial \bar{E}_{ij}}{\partial v} = \frac{0.6023}{R_{yij}/R_{xij}}\frac{\partial (R_{yij}/R_{xij})}{\partial v}. \tag{C.14}$$

The expressions about $\partial K_{oj}/\partial v$ are analogous to the above equations when all subscripts i in those equations are shifted with subscript o. The only difference between $\partial K_{ij}/\partial v$ and $\partial K_{oj}/\partial v$ is as follows:

$$\frac{\partial (R_{yij}/R_{xij})}{\partial v} = -\frac{2r_i D_b D_p \sin\alpha_{ij}}{(2r_i - D_b)(D_p - D_b\cos\alpha_{ij})^2}\frac{\partial \alpha_{ij}}{\partial v}, \tag{C.15}$$

$$\frac{\partial (R_{yoj}/R_{xoj})}{\partial v} = -\frac{2r_o D_b D_p \sin\alpha_{oj}}{(2r_i - D_b)(D_p + D_b\cos\alpha_{oj})^2}\frac{\partial \alpha_{oj}}{\partial v}, \tag{C.16}$$

$$\frac{\partial \bar{R}_{ij}}{\partial v} = \frac{2r_i^2 D_b^2 D_p \sin\alpha_{ij}}{[(2r_i - D_b)(D_p - D_b\cos\alpha_{ij}) + 2r_i D_p]^2}\frac{\partial \alpha_{ij}}{\partial v}, \tag{C.17}$$

$$\frac{\partial \bar{R}_{oj}}{\partial v} = \frac{2r_o^2 D_b^2 D_p \sin\alpha_{oj}}{[(2r_o - D_b)(D_p + D_b\cos\alpha_{oj}) + 2r_o D_p]^2}\frac{\partial \alpha_{oj}}{\partial v}. \tag{C.18}$$

The partial derivatives of the centrifugal force with respect to the displacement can be calculated from

$$\frac{\partial F_{ej}}{\partial v_{rj}} = m_b\omega_{mj}\left[(D_p + 2v_{rj})\frac{\partial \omega_{mj}}{\partial v_{rj}} + \omega_{mj}\right], \tag{C.19}$$

$$\frac{\partial F_{ej}}{\partial v_{zj}} = m_b\omega_{mj}(D_p + 2v_{rj})\frac{\partial \omega_{mj}}{\partial v_{zj}}. \tag{C.20}$$

Other unknown partial derivatives with respect to v, which denotes v_{rj} or v_{zj}, can be expressed as follows:

$$\frac{\partial M_{gj}}{\partial v} = 0.1 m_b D_b^2\left(\omega_{bj}\sin\beta_j\frac{\partial \omega_{mj}}{\partial v} + \omega_{mj}\sin\beta_j\frac{\partial \omega_{bj}}{\partial v} + \omega_{mj}\omega_{bj}\cos\beta_j\frac{\partial \beta_j}{\partial v}\right), \tag{C.21}$$

Inner race control:

$$\frac{\partial \beta_j}{\partial v} = \frac{1-\gamma\cos\alpha_{ij}}{1+\gamma^2-2\gamma\cos\alpha_{ij}}\frac{\partial \alpha_{ij}}{\partial v}, \tag{C.22}$$

$$\frac{\partial \omega_{mj}}{\partial v} = \omega_i\frac{-(1+\gamma\cos\alpha_{oj})\sin(\alpha_{ij}-\alpha_{oj})(\partial\alpha_{ij}/\partial v) + [\gamma\sin\alpha_{ij} + \gamma\sin\alpha_{oj} + \sin(\alpha_{ij}-\alpha_{oj})](\partial\alpha_{oj}/\partial v)}{[1+\cos(\alpha_{ij}-\alpha_{oj})]^2}, \tag{C.23}$$

$$\frac{\partial \omega_{bj}}{\partial v} = -\omega_i\frac{H_1(\partial\alpha_{ij}/\partial v) + H_2(\partial\alpha_{oj}/\partial v) + H_3(\partial\beta_j/\partial v)}{\gamma\cos\beta_j[1+\cos(\alpha_{ij}-\alpha_{oj})]^2}, \tag{C.24}$$

$$H_1 = -(1+\gamma\cos\alpha_{oj})[\sin\alpha_{ij} + \sin\alpha_{oj} + \gamma\sin(\alpha_{ij}-\alpha_{oj})], \tag{C.25}$$

$$H_2 = -(\cos\alpha_{ij} - \gamma)[\gamma \sin\alpha_{ij} + \gamma \sin\alpha_{oj} + \sin(\alpha_{ij} - \alpha_{oj})], \tag{C.26}$$

$$H_3 = \tan\beta_j(\cos\alpha_{ij} - \gamma)(1 + \gamma\cos\alpha_{oj})[1 + \cos(\alpha_{ij} - \alpha_{oj})], \tag{C.27}$$

Outer race control:

$$\frac{\partial\beta_j}{\partial v} = \frac{1 + \gamma\cos\alpha_{oj}}{1 + \gamma^2 + 2\gamma\cos\alpha_{oj}}\frac{\partial\alpha_{oj}}{\partial v}, \tag{C.28}$$

$$\frac{\partial\omega_{mj}}{\partial v} = \omega_i\frac{[\gamma\sin\alpha_{ij} + \gamma\sin\alpha_{oj} + \sin(\alpha_{ij} - \alpha_{oj})](\partial\alpha_{ij}/\partial v) - (1 - \gamma\cos\alpha_{ij})\sin(\alpha_{ij} - \alpha_{oj})(\partial\alpha_{oj}/\partial v)}{[1 + \cos(\alpha_{ij} - \alpha_{oj})]^2}, \tag{C.29}$$

$$\frac{\partial\omega_{bj}}{\partial v} = -\omega_i\frac{H_1(\partial\alpha_{ij}/\partial v) + H_2(\partial\alpha_{oj}/\partial v) + H_3(\partial\beta_j/\partial v)}{\gamma\cos\beta_j[1 + \cos(\alpha_{ij} - \alpha_{oj})]^2}, \tag{C.30}$$

$$H_1 = (\cos\alpha_{oj} + \gamma)[\gamma\sin\alpha_{ij} + \gamma\sin\alpha_{oj} + \sin(\alpha_{ij} - \alpha_{oj})], \tag{C.31}$$

$$H_2 = -(1 - \gamma\cos\alpha_{ij})[\sin\alpha_{ij} + \sin\alpha_{oj} + \gamma\sin(\alpha_{ij} - \alpha_{oj})], \tag{C.32}$$

$$H_3 = \tan\beta_j(\cos\alpha_{oj} + \gamma)(1 - \gamma\cos\alpha_{ij})[1 + \cos(\alpha_{ij} - \alpha_{oj})]. \tag{C.33}$$

References

[1] H. Perret, Elastische Spielschwingungen konstant belasteter Wälzlager, *Werkstatt und Betrieb* 83 (1950) 354–358.
[2] E. Meldau, Die Bewegung der Achse von Wälzlagern bei geringen Drehzahlen, *Werkstatt und Betrieb* 84 (1951) 308–313.
[3] A.B. Jones, A general theory of elastically constrained ball and radial roller bearings under arbitrary load and speed conditions, *ASME Journal of Basic Engineering* 82 (1960) 309–320.
[4] T.A. Harris, *Rolling Bearing Analysis*, second ed., Wiley, New York, 1984.
[5] C.T. Walters, The dynamics of ball bearings, *ASME Journal of Lubrication Technology* 93 (1971) 1–10.
[6] P.L. Gupta, Dynamics of rolling element bearings, Parts I to IV, *ASME Journal of Lubrication Technology* 101 (1979) 293–326.
[7] O.G. Gutafsson, T. Tallian, et al., Research report on study of the vibration characteristics of bearings, Report: AL631023, Reg: 585 14:4223 SKF Ind., Inc., 1963.
[8] T. Yamamoto, On the vibration of a shaft supported by bearing having radial clearance, *Transactions of the Japanese Society of Mechanical Engineering* 21 (1955) 182–192.
[9] D.W. Childs, Fractional frequency rotor motion due to clearance effects, *ASME Journal of Engineering for Power* 104 (1982) 533–536.
[10] S. Saito, Calculation of non-linear unbalance response of horizontal Jeffcott rotors supported by ball bearings with radial clearances, *ASME Journal of Vibration, Acoustics, Stress, Reliability and Designs* 107 (1985) 416–420.
[11] B. Mevel, J.L. Guyader, Routes to chaos in ball bearings, *Journal of Sound and Vibration* 162 (1993) 471–487.
[12] M. Tiwari, K. Gupta, O. Prakash, Effect of radial internal clearance of a ball bearing on the dynamics of a balanced horizontal rotor, *Journal of Sound and Vibration* 238 (2000) 723–756.
[13] M. Tiwari, K. Gupta, O. Prakash, Dynamic response of an unbalanced rotor supported on ball bearings, *Journal of Sound and Vibration* 238 (2000) 757–779.
[14] S.P. Harsha, K. Sandeep, R. Prakash, The effect of speed of balanced rotor on nonlinear vibrations associated with ball bearings, *International Journal of Mechanical Science* 45 (2003) 725–740.
[15] J.M. de Mul, J.M. Vree, D.A. Maas, Equilibrium and associated load distribution in ball and roller bearings loaded in five degrees of freedom while neglecting friction—Part I: general theory and application to ball bearings, *ASME Journal of Tribology* 111 (1989) 142–148.
[16] A. Liew, N. Feng, E.J. Hahn, Transient rotordynamic modeling of rolling element bearing systems, *ASME Journal of Engineering for Gas Turbines and Power* 124 (2002) 984–991.
[17] T.E. Tallian, O.G. Gustafsson, Progress in rolling bearing vibration research and control, *ASLE Transactions* 8 (1965) 195–207.
[18] E.M. Yhland, Waviness measurement—an instrument for quality control in rolling bearing industry, *Proceedings of the Institution of Mechanical Engineering* 182 (Part 3K) (1967) 438–445.
[19] F.P. Wardle, S.Y. Poon, Rolling bearings noise, cause and cure, *Chartered Mechanical Engineering* (July/August) (1983) 36–40.
[20] F.P. Wardle, Vibration forces produced by waviness of the rolling surfaces of thrust loaded ball bearing, Part 1: theory, *Proceedings of the Institution of Mechanical Engineers* 202 (C5) (1988) 305–312.
[21] F.P. Wardle, Vibration forces produced by waviness of the rolling surfaces of thrust loaded ball bearing, Part 1: experimental validation, *Proceedings of the Institution of Mechanical Engineers* 202 (C5) (1988) 313–319.

[22] E. Yhland, A linear theory of vibrations caused by ball bearings with form errors operating at moderate speed, *ASME Journal of Tribology* 114 (1992) 348–359.
[23] N. Aktüuk, The effect of waviness on vibrations associated with ball bearings, *ASME Journal of Tribology* 121 (1999) 667–676.
[24] G.H. Jang, S.W. Jeong, Nonlinear excitation model of ball bearing waviness in a rigid rotor supported by two or more ball bearings considering five degrees of freedom, *ASME Journal of Tribology* 124 (2002) 82–90.
[25] G.H. Jang, S.W. Jeong, Analysis of a ball bearing with waviness considering the centrifugal force and gyroscopic moment of the ball, *ASME Journal of Tribology* 125 (2003) 487–498.
[26] D.E. Brewe, B.J. Hamrock, Simplified solution for elliptical-contact deformation between two elastic solids, *Journal of Lubrication Technology* 99 (1977) 485–487.
[27] B.J. Hamrock, D. Dowson, *Ball Bearing Lubrication—The Elastohydrodynamics of Elliptical Contacts*, Wiley, New York, 1981.
[28] P.K. Gupta, *Advanced Dynamics of Rolling Elements*, Wiley, New York, 1984.
[29] J.Q. Zhou, Y.Y. Zhu, *Nonlinear Vibrations*, Xi'an Jioatong University Press, China, 1998.